Development of the CMA-GFS-AERO 4D-Var assimilation system v1.0- Part 1: System description and preliminary experimental results

Yongzhu Liu[1,2,3], Xiaoye Zhang[2,4], Wei Han[1,2,3], Chao Wang[1,2,3], Wenxing Jia[2,4], Deying Wang[2,4], Zhaorong Zhuang[1,2,3], Xueshun Shen[1,2,3]

[1]CMA Earth System Modeling and Prediction Centre, China Meteorological Administration, Beijing, 10081, China
[2]State Key Laboratory of Severe Weather, China Meteorological Administration, Beijing, 10081, China
[3]Key Laboratory of Earth System Modeling and Prediction China Meteorological Administration, China Meteorological Administration, Beijing, 10081, China
[4]Key Laboratory of Atmospheric Chemistry of CMA, Chinese Academy of Meteorological Sciences, Beijing, 10081, China

Correspondence to: Xiaoye Zhang (xiaoye@cma.gov.cn), Xueshun Shen (shenxs@cma.gov.cn)

Abstract. We developed a strongly coupled aerosol-~~chemistry~~ meteorology four-dimensional variational (4D-Var) assimilation system, CMA-GFS-AERO 4D-Var, for investigating the feedbacks of chemical data assimilation on meteorological forecasts. This system was developed on the basis of the framework of the incremental analysis scheme of the China Meteorological Administration Global Forecasting System (CMA-GFS). CMA-GFS-AERO 4D-Var includes three component models: forward, tangent linear, and adjoint models. CMA-GFS-AERO forward model was constructed by integrating an aerosol module containing main physical processes of black carbon (BC) aerosol in the atmosphere into the CMA-GFS weather model. The tangent linear and the adjoint of the aerosol module was further developed and coupled online with the CMA-GFS tangent linear and adjoint models, respectively. In CMA-GFS-AERO 4D-Var, the BC mass concentration was used as the control variable and minimized together with atmospheric variables. The validation of this system includes the tangent linear approximation, the adjoint correctness test, the single-~~point~~ observation ~~ideal~~ experiment and the full observation experiment. The results show that CMA-GFS-AERO tangent linear model performs well in tangent linear approximation for BC, and adjoint sensitivity agrees well with tangent linear sensitivity. Assimilating BC observations can generate analysis increments not only for BC but also for atmospheric variables, highlighting the capability of CMA-GFS-AERO 4D-Var in exploring the feedback ~~effect~~ of BC assimilation on atmospheric variables. The computational performance of CMA-GFS-AERO 4D-Var also indicates the potential in operational application. This study focuses on the theoretical architecture and practical implementation of the system, the detailed analysis of the batch test will be described in part 2 of this paper.

1 Introduction

Coupled chemistry meteorology models (CCMM) are atmospheric chemistry models that concurrently simulate meteorological processes and chemical transformations (Zhang, 2008; Baklanov et al., 2014; Bocquet, 2015). They are more

recent compared to chemical transport models (CTM), which rely on meteorological fields as inputs (Seinfeld and Pandis, 1998). ~~Moisture and temperature perturbations to dynamics resulting from aerosol microphysics and radiative forcing are taken into consideration by CCMM,~~ CCMM account for the feedback mechanism between aerosols and meteorology, specifically the moisture and temperature perturbations resulting from aerosol microphysics and radiative forcing, which, in turn, affect atmospheric dynamics such as convection, circulation, and stability, whereas CTM~~s~~ lack the capability to incorporate these feedback~~s~~ mechanisms (Guerrette and Henze, 2015).

CCMM provide~~s~~ the possibility to assimilate both meteorological and chemical data, enabling the production of an optimal initial condition for~~enabling to produce the optimal initial values for~~ improving air quality predictions and developing re-analysis of three-dimensional (3D) chemical concentrations over the past decades (Bocquet, 2015). One of the first applications of data assimilation with a CCMM was conducted at Météo-France. Semane et al. (2009) used four-dimensional variational (4D-Var) data assimilation to assimilate the vertical profiles of ozone (O_3) concentrations obtained from the Microwave Limb Sounder (MLS) aboard the Aura satellite ~~AURA/MLS~~ into the ARPEGE/MOCAGE (Action de Recherche Petite Echelle Grande Echelle/Modèle de Chimie Atmosphérique de Grande Echelle) chemistry meteorology integrated system, and found that the assimilation of O_3 reduces the wind bias in the lower stratosphere. This general approach is also adopted by the European Centre for Medium-range Weather Forecasts (ECMWF), although without considering the influence of chemical species on meteorological variables (Flemming et al.,2011; Inness et al., 2013). Flemming et al. (2011) utilized the 4D-Var system of the Integrated Forecast System (IFS) coupled with three different O_3 chemistry mechanisms, including a linear chemistry, the MOZART3 (Model for Ozone and Related Chemical Tracers, version 3) chemistry, and the TM5 (Transport Model, version 5) chemistry, to assimilate O_3 data from four satellite-borne sensors to improve the simulation of the stratospheric O_3 hole in 2008. ~~Inness et al. (2013) used 4D-Var system of IFS coupled with the MOZART3 CTM to produce re-analysis of atmospheric concentrations of four chemical species, including CO, NO_x, O_3, and formaldehyde (HCHO), over an 8-year period, and the data assimilation results showed notable improvements for CO and O_3, but little effect for NO_2, because of its shorter lifetime compared to those of CO and O_3.~~ Previous efforts have also explored the application of ensemble-based methods for data assimilation with a CCMM (Pagowski and Grell, 2012; Bocquet et al., 2015). Pagowski and Grell (2012) assimilated surface measurements of fine aerosols using the Weather Research and Forecasting-Chemistry model (WRF-Chem) and the Ensemble Kalman filter (EnKF) method. Bocquet et al. (2015) also presented an application of the EnKF to assimilate surface fine particulate matter observations and meteorological observations with the WRF-Chem model over the eastern part of North America. Results demonstrated that a large positive impact of aerosol data assimilation on aerosol concentrations, while the effect of meteorological observation assimilation on aerosol concentration is rather minor. All the preceding studies have laid good foundations for data assimilation with CCMM. However, since CCMM are fairly recent, the development and applications of data assimilation in

CCMM are still limited. Further research and more attention are required, especially in terms of the potential feedbacks of chemical data assimilation on meteorological forecasts. Additionally, EnKF estimates background error covariance through ensemble forecasts, which rely on a limited number of ensemble members (Zhu et al., 2022). In high-dimensional problems, the limited number of samples may not be able to fully capture all the error characteristics, resulting the inaccurate of the estimation of background error covariance. In contrast, 4D-Var generally offers higher accuracy for high-dimensional problems by incorporating both the full observational data and model dynamics within the assimilation window, resulting in more precise state estimation. While the flow dependence of the background error covariance is implicitly realized within the assimilation window in 4D-Var, modeling the cross-variable component of the covariance presents a significant challenge in data assimilation for CCMM. Furthermore, the tangent linear model (TLM) and the adjoint model (ADM) are essential components of 4D-Var, but their development is often fraught with difficulties.

~~As a method widely used by major~~international ~~mainstream numerical~~ weather ~~prediction centers, 4D-Var is considered superior to three-dimensional variational (3D-Var) data assimilation, which ignores the time distribution of observations and assumes that observations within a time window are concentrated at the analysis moment (Lorenc and Rawlins, 2010). 4D-Var is an extension of 3D-Var in the time dimension, it can consider the observation time more accurately and can implicitly propagate the initial background error covariance during the assimilation window (Lorenc and Rawlins, 2010). In the development of 4D-Var, the adjoint model (ADM) plays a crucial role by offering the sensitivity and gradient of the cost function with respect to the control variables.~~ Significant efforts have been made in the field of atmospheric chemistry adjoint modeling. Elbern and Schmidt (1999) first constructed the ADM of a 3D CTM, EUARD (The University of Cologne European Air Pollution Dispersion Chemistry Transport Model~~EUARD~~) ~~for the first time~~. Inspired by this work, various ADM of CTM have been successively developed, mainly including CHIMERE (Menut et al., 2000; Vautard et al., 2000; Schmidt and Martin, 2003), IMAGES (Intermediate Model of Global Evolution of Species; Müller and Stavrakou, 2005), STEM-III (Sulfur Transport Eulerian Model; Sandu et al., 2005), CAMx (Comprehensive Air Quality Model with Extensions model; Liu, 2005), CMAQ (Community Multiscale Air Quality model; Hakami et al., 2007) and GEOS-Chem (Henze et al., 2007). An et al. (2016) and Wang et al. (2022) constructed the ADM of GRAPES-CUACE (Global/Regional Assimilation and PrEdiction System coupled with CMA Unified Atmospheric Chemistry Environmental Forecasting System), an independently developed CCMM in China (Wang et al., 2010, 2018). ADM of these widely used CTM play an important role in inverse modelling and chemical data assimilation (Menut et al., 2000; Müller and Stavrakou, 2005; Sandu et al., 2005; Hakami et al., 2007; Henze et al., 2009). However, these CTM do not take into account the influence between chemical species and meteorological variables, resulting in certain uncertainties in adjoint sensitivity, which in turn affects the

effectiveness of 4D-Var. Although GRAPES-CUACE is a CCMM, its ADM only includes the adjoint of the chemical model and not the adjoint of the meteorological model, leading to uncertainties in the sensitivity calculation as well.

Black carbon (BC) aerosol, a major component of the fine particulate matter ~~is one of the major components of (~~$PM_{2.5}$~~),~~ defined by an aerodynamic diameter of 2.5 micrometers or less, primarily originates ~~mainly~~ from the incomplete combustion of biomass and fossil fuels (Kuhlbusch, 1998). As an important atmospheric pollutant, BC is porous and adsorbs other solid and gaseous pollutants (e.g., SO_2, O_3, etc.), and provides catalytic conditions for them, which plays an important role in photochemical and heterogeneous reactions and gas-particle conversion processes (Koch, 2001). BC is also the main optically absorbing component of atmospheric aerosols, effectively absorbing solar radiation in the visible to infrared wavelength range, thus affecting not only the surface temperature but also the 3D temperature field. The climatic effects of BC have been widely reported, but the extent to which it affects weather forecasting requires further investigation (Chung and Seinfeld, 2002; Menon et al., 2002; Bond et al., 2013).

To deeply investigate the feedbacks of aerosol~~chemical~~ data assimilation on meteorological forecasts, we utilized BC as a starting point to develop the strongly coupled aerosol-~~chemistry~~ meteorology 4D-Var system. Firstly, we constructed a coupled aerosol-meteorology~~CCMM~~ system, named CMA-GFS-AERO, by integrating an aerosol module (AERO-BC) containing main aerosol physical processes of BC in the atmosphere into the operational version of the weather model CMA-GFS V4.0 (Shen et al., 2023), which was developed by the China Meteorological Administration (CMA). Then, the tangent linear and the adjoint of the AERO-BC module was constructed and coupled online with the ~~tangent linear model (~~TLM~~)~~ and ADM of CMA-GFS (Liu et al., 2017, 2023; Zhang et al., 2019), respectively. Thus, CMA-GFS-AERO ADM includes not only the adjoint of physical processes of BC, but also the adjoint of the meteorological model. Moreover, the BC adjoint variables and the meteorological adjoint variables mutually influence each other throughout the adjoint integration process, leading to a notable enhancement in the precision of adjoint sensitivity of ~~chemistry~~ aerosol and meteorology state. Based on the CMA-GFS-AERO forward model ~~CCMM~~ and its TLM and ADM, we further constructed the CMA-GFS-AERO 4D-Var by ~~adding the control variable of BC into~~adding BC as a control variable into the incremental analysis scheme of CMA-GFS 4D-Var. The rationality and capability of CMA-GFS-AERO 4D-Var in capturing the feedbacks of chemical data assimilation on meteorological analysis were verified using the single~~-point~~ observation ~~ideal~~ experiment and the full observation experiment. The following part is divided into four sections. Section 2 introduces the methods, Section 3 describes the development of CMA-GFS-AERO 4D-Var, Section 4 provides the model setup, Section 5~~4~~ presents the results, and the conclusions are found in Section 6~~5~~.

2 Methodology

2.1 Model description

2.1.1 CMA-GFS

The China Meteorological Administration Global Forecasting System (CMA-GFS, formerly known as GRAPES-GFS) is an operational global numerical weather model independently developed by the CMA (Chen and Shen, 2006; Chen et al., 2008; Shen et al., 2023). For this work, we used CMA-GFS version 4.0 (CMA-GFS v4.0). The dynamic core of CMA-GFS utilizes the fully compressible non-hydrostatical equations formulated on spherical coordinate with latitude and longitude, and adopts the height-based, terrain-following coordinate which is shown in Fig. S1 (Yang et al., 2007) . The model employs semi-implicit and semi-Lagrangian in two-level time integration (Yang et al., 2007). The spatial differential adopts Arakawa-C grid in the horizontal, and Charney-Philips variable staggering in the vertical. The large-scale transport processes utilize a hybrid Piecewise Rational Method (PRM) and Quasi-Monotone Semi-Lagrangian (QMSL) scheme (Su et al., 2013). ~~The physical parameterization schemes are freely combinable, which principally include cumulus convection, microphysical precipitation, radiative transfer, land surface and boundary layer processes.~~ The physical parameterization schemes used in this work mainly include the Simplified Arakawa Schubert (SAS) cumulus convection scheme (Arakawa and Schubert, 1974; Liu et al., 2015), the double-moment cloud microphysics scheme (Liu et al., 2003a, 2003b; Li et al., 2024), the Rapid Radiative Transfer Model for the GCM (RRTMG) longwave and shortwave radiation schemes (Mlawer et al., 1997; Morcrette et al., 2008), the Common Land Model (CoLM) land surface scheme (Dai et al., 2003), and the New Medium Range Forecast (NMRF) boundary layer scheme (Hong and Pan, 1996; Han and Pan, 2011). The state variables of the CMA-GFS nonlinear model (NLM) include non-dimensional pressure (π), potential temperature (θ), the east-west component of horizontal wind (u), the north-south component of horizontal wind (v), the vertical component of wind ($\widehat{w}$), and the specific humidity (q).

2.1.2 CUACE

CUACE (CMA Unified Atmospheric Chemistry Environmental Forecasting System) is an air quality model developed by the Chinese Academy of Meteorological Sciences to study both air quality forecasting and climate change (Gong and Zhang, 2008; Wang et al., 2010; Zhou et al., 2012). CUACE mainly includes three modules: the aerosol module, the gaseous chemistry module and the thermodynamic equilibrium module. CUACE adopts CAM (Canadian Aerosol Module; ~~(~~Gong et al., 2003~~)~~), which employs the size-segregated multicomponent aerosol algorithm, as its aerosol module. CAM involves six types of aerosols: BC, sulfate (SF), nitrate (NI), sea salt (SS), organic carbon (OC) and soil dust (SD), and each of them utilizes the sectional representation method (Gelbard et al., 1980; Meng et al., 1998; Gong et al., 2003), in which the aerosol size distribution is generally approximated by a set of contiguous, nonoverlapping and discrete size bins, to represent particle

size distributions. The core of CAM is the major aerosol processes in the atmosphere, including hygroscopic growth, coagulation, nucleation, condensation, dry deposition/sedimentation, and below-cloud scavenging.

2.2 Incremental 4D-Var

The CMA-GFS 4D-Var data assimilation system has been in operation at CMA since 1 July 2018 (Zhang et al., 2019). CMA-GFS 4D-Var applies the incremental analysis scheme proposed by Courtier et al. (1994). The cost function is defined as

$$J(\delta x) = \frac{1}{2}\delta x^T \mathbf{B}^{-1}\delta x + \frac{1}{2}\sum_{i=0}^{n}(\mathbf{H}_i\mathbf{M}_{0\to i}\delta x + d_i)^T\mathbf{R}_i^{-1}(\mathbf{H}_i\mathbf{M}_{0\to i}\delta x + d_i) + J_c, \quad (1)$$

where $\delta x = x_a - x_b$ represents the analysis increment of the model variables, x_a is the analysis ~~filed~~field, x_b is the background state, $d_i = \boldsymbol{H}_i\boldsymbol{M}_{0\to i}(x_b) - y_i$ is the observation innovation~~increment~~ at time i, y_i is the observation at time i, $\boldsymbol{H}_i$ represents the observation operator at time i, $\boldsymbol{M}_{0\to i}$ denotes the model integration from the analysis time to time i, $\mathbf{H}_i$ is the linear operator corresponding to $\boldsymbol{H}_i$, $\mathbf{M}_{0\to i}$ is the linear model~~operator~~ corresponding to $\boldsymbol{M}_{0\to i}$, $\mathbf{B}$ represents the error covariance matrix of x_b, $\mathbf{R}_i$ denotes the observation error covariance matrix at time i, and J_c is the weak constraint term on the basis of the digital filter. J_c is not relevant to the current work, so the formula described below omits J_c term from the cost function for the sake of simplicity.

After the physical and preconditioning transformations of the control variables, the cost function can be expressed as (Courtier et al., 1994; Lorenc et al., 2000; Zhang et al., 2019)

$$J(w) = \frac{1}{2}w^{\mathrm{T}}w + \frac{1}{2}\sum_{i=0}^{n}(\mathbf{H}_i\mathbf{M}_{0\to i}Uw + d_i)^T\mathbf{R}_i^{-1}(\mathbf{H}_i\mathbf{M}_{0\to i}Uw + d_i), \quad (2)$$

where w denotes the control variables after the physical and preconditioning transformations, and the analysis increment is expressed as $\delta x = Uw$, U $(UU^T = \mathbf{B})$ is the square root matrix of the background error covariance matrix ~~after the physical and preconditioning transformations~~.

The gradient of the cost function $J(w)$with respect to the control variable w is

$$\nabla_w J = w + \sum_{i=0}^{n} U^T\mathbf{M}_{0\to i}^T\mathbf{H}_i^T\mathbf{R}_i^{-1}(\mathbf{H}_i\mathbf{M}_{0\to i}Uw + d_i), \quad (3)$$

where $\mathbf{H}_i^T$ is the adjoint operator of $\mathbf{H}_i$, and $\mathbf{M}_{0\to i}^T$ is the adjoint ~~operator~~ model of $\mathbf{M}_{0\to i}$, which denotes the backward~~inverse~~ integration of the ADM from the time i to the analysis time.

Currently, the CMA-GFS 4D-Var system adopts a 6-h cycle and is performed four times a day, with assimilation windows of 0300 UTC-0900 UTC, 0900 UTC-1500 UTC, 1500 UTC-2100 UTC and 2100 UTC-0300 UTC. The assimilation process is divided into two parts: the outer loop and the inner loop. In the outer loop, the CMA-GFS NLM ($\boldsymbol{M}_{0\to i}$) is integrated at high resolution for 6 hours to obtain the trajectory, which is a collection of stored values of all model state variables at all time steps within the assimilation window. The observation innovation ~~increment~~ d_i is calculated in the outer loop as well. In the inner loop, the CMA-GFS TLM and ADM are integrated at low resolution to calculate the cost function ($J(w)$) and its

gradient ($\nabla_w J$). The gradient is further provided to the Lanczos-CG algorithm (Lanczos, 1950; Liu et al., 2018) to perform the minimization, obtaining the optimal analysis increments to control variables.

3 Development of CMA-GFS-AERO 4D-Var

The computational cost is an important factor to be considered when developing a coupled aerosol~~chemistry~~ meteorology 4D-Var system with potential for operational application (Flemming et al., 2015). The CUACE model is computationally expensive since it includes more than one hundred chemical variables for aerosols and gases, as well as hundreds of gas-phase chemical reactions. It is difficult to construct a coupled aerosol-~~chemistry~~ meteorology 4D-Var system directly based on the CUACE model. On the other hand, BC has an important impact on the climate and can be used to study the two-way feedback interactions between aerosol~~chemistry~~ and meteorology (Chung and Seinfeld, 2002; Menon et al., 2002; Bond et al., 2013). Therefore, we utilized BC as a starting point to construct the strongly coupled aerosol-~~chemistry~~ meteorology 4D-Var system (CMA-GFS-AERO 4D-Var).

Creating CMA-GFS-AERO 4D-Var required three important components: (1) CMA-GFS-AERO forward model, (2) CMA-GFS-AERO TLM and ADM, and (3) 4D-Var framework. This section provides a detailed description of the construction of the CMA-GFS-AERO 4D-Var from these three aspects.

3.1 CMA-GFS-AERO ~~CCMM~~forward model

In this work, for the sake of interest in BC and the consideration of computational efficiency, we developed the CMA-GFS-AERO forward model by integrating the aerosol module AERO-BC into CMA-GFS v4.0. The AERO-BC module was created by extracting BC-related codes from the CUACE model, with its functionality aligning with the BC aerosol processes in the CAM module of CUACE. In other words, the physical processes for BC in AERO-BC are identical to those in the CAM module, with no changes made. The main differences lie in the engineering aspect: (1) while the CAM module was originally written in Fortran 77, the AERO-BC code has been rewritten in Fortran 90; (2) since CAM in CUACE deals with six types of aerosols, the code structure is somewhat complex and redundant, whereas AERO-BC focuses solely on BC, resulting in a simpler and more streamlined structure. These updates improve code readability and enhance computational efficiency, without affecting the underlying physical processes.~~we extracted the codes related to BC from the CUACE model and converted them from Fortran 77 format to Fortran 90 format. Meanwhile, we also optimized the program structure and interface scalability, making it easier to be developed into tangent linear and adjoint codes. The resulting aerosol module is referred to as AERO-BC. The AERO-BC includes 18 subroutines in total: 1 emission flux program (sf_bc), 4 vertical diffusion programs (trac_vert_diff and its subroutines), 6 programs related to the aerosol physical processes of BC as mentioned in Section 2.1.2 (aerosol_bc and its subroutines), and 7 programs related to the constant

definitions and the parameter calculations. We further integrated the AERO-BC into CMA-GFS v4.0 by constructing interface programs (black_carbon and bc_driver). Thus, we obtained the CMA-GFS-AERO CCMMforward model. The structure of the CMA-GFS-AERO model is shown in Fig. S2.

In the AERO-BC, BC is represented by 6 bins with particle diameters of 0.01-0.04, 0.04-0.16, 0.16-0.64, 0.64-2.56, 2.56-10.24, and 10.24-40.96 μm, where the radius range is calculated by the geometric progression method to satisfy $i = 1 + \ln[(r_i/r_1)^3]/\ln[V_{RAT}]$, and V_{RAT} is the average volume ratio between adjacent bins (Jacobson et al., 1994). Thus, six new prognostic variables for the mass mixing ratio of BC, denoted as ψ_{bc}–ψ_{bc}^{n}(unit: kg/kg), where $n = 1, ..., 6$, are added in the dynamical framework of CMA-GFS.

The main processes in AERO-BC include: (1) calculating the emission flux of BC through the surface flux calculation module, (2) calculating the vertical diffusion trend of BC by solving the vertical diffusion equation, and (3) simulating key BC aerosol processes in the atmosphere, including hygroscopic growth, coagulation, nucleation, condensation, dry deposition/sedimentation, and below-cloud scavenging. For more details, please refer to the relevant literature on the CAM module (Gong et al., 2003; Gong and Zhang et al., 2008; Wang et al., 2010; Zhou et al., 2012). In the integration of AERO-BC with CMA-GFS, the interface programs transfer meteorological parameters (e.g., temperature, wind, and humidity) from CMA-GFS to AERO-BC, extend the spatial dimension from 1-D to 3-D, and read emissions for AERO-BC.

The transport processes for $\psi_{bc}^{n}\psi_{bc}$ are the same as that those for the variables associated with the different water species water-matter variables in CMA-GFS, using the hybrid PRM and QMSL schemes (Su et al., 2013).

Besides, according to the vertical distribution characteristics of BC in the MERRA-2 (Modern-Era Retrospective analysis for Research and Applications, Version 2) reanalysis data (https://daac.gsfc.nasa.gov), we observed that the BC mass mixing ratio decreases rapidly in magnitude after entering the stratosphere, reaching values ofto about 10^{-12} kg/kg., Thiswhich is 2-3 orders of magnitude smaller relative compared to the surface.. To improve computational efficiency and balance memory usage with the effectiveness of BC forecasting, we set the height of $\psi_{bc}^{n}\psi_{bc}$ in the CMA-GFS-AERO model to 65 levels (approximatelyabout 30 hPa), which corresponds to the middle layer of the stratosphereapproximately the middle layer of the stratosphere, to improve calculation efficiency and balance the memory usage and the effectiveness of BC forecast. Regarding the absence of BC above model level 65, we handled vertical transport by assuming that any BC concentrations above this level are negligible. This approximation does not significantly affect the model's performance, as the BC mass mixing ratio is very small in the upper layers. Correspondingly, in the adjoint code, BC concentrations above model level 65 are also treated as negligible, and this does not significantly affect the adjoint calculations.

3.2 CMA-GFS-AERO TLM and ADM

In developing the TLM and ADM of the CMA-GFS-AERO model, we firstly constructed the tangent linear and adjoint codes of the AERO-BC module, subsequently coupled them with the TLM and ADM of CMA-GFS model (Liu et al., 2017,

2023; Zhang et al., 2019), respectively. Since adjoint codes generated by automatic differentiation tools often suffer from issues such as poor readability and maintainability, low efficiency and even errors due to the complexity of numerical models (Zou et al., 1997), the~~The~~ tangent linear and adjoint codes in this study were written line-by-line manually, without using any automatic differentiation tool.

The AERO-BC can be symbolically written as

$$Y = \boldsymbol{F}(C) \quad , \tag{4}$$

where $\boldsymbol{F}$ denotes the AERO-BC model operator, C and Y are vectors representing the input and output variables of the AERO-BC, respectively.

The TL of the AERO-BC can be obtained by linearizing $\boldsymbol{F}$, expressed as

$$\delta Y = \mathbf{F}\delta C = \frac{\partial \boldsymbol{F}}{\partial C}\delta C, \tag{5}$$

where $\mathbf{F}$ is the TL model operator, δC and δY represent perturbations of input and output variables of the AERO-BC, respectively.

~~The AERO-BC TL contains the tangent linear programs corresponding to the emission flux, vertical diffusion, and aerosol physical processes as mentioned in Section 3.1. We further integrated the AERO-BC TL into the CMA-GFS TLM by constructing the interface program (tl_black_carbon and tl_bc_driver). The tangent linear of BC transport processes is the same as that for the water-matter variables in CMA-GFS TLM, using the tangent linear of QMSL. Thus, we obtained the CMA-GFS-AERO TLM.~~

The adjoint of the AERO-BC is essentially the transpose of the AERO-BC TL, expressed as

$$\delta C^* = \mathbf{F}^T \delta Y^*, \tag{6}$$

where $\mathbf{F}^T$ is the adjoint operator of $\mathbf{F}$, δY^* and δC^* represent input and output variables of the adjoint of AERO-BC, respectively.

In constructing the TL and the adjoint of AERO-BC, no simplifications were made to the AERO-BC processes. Specifically, no regularization was applied to the nonlinear equations, nor were any complex processes, which were difficult to linearize, omitted. As a result, the TL and the adjoint of AERO-BC fully include all processes related to emission flux, vertical diffusion, and aerosol physical processes as described in Section 3.1.

The TL and the adjoint of AERO-BC are 1-D modules with fixed latitude and longitude coordinates. To extend them to 3-D, the tangent linear and the adjoint of the interface programs were also constructed. Furthermore, the tangent linear and the adjoint of BC transport processes follow the same framework as those for the variables associated with the different water species in the CMA-GFS TLM and ADM, utilizing the tangent linear and the adjoint of QMSL. In this way, the 3-D parameters could be transferred from CMA-GFS to AERO-BC. Thus, we obtained the CMA-GFS-AERO TLM and ADM.

~~The adjoint of AERO-BC, which includes the adjoint of the emission flux (ad_sf_bc), the adjoint of the vertical diffusion (ad_trac_vert_diff and its subroutines), and the adjoint of aerosol physical processes of BC (ad_aerosol_bc and its subroutines), was coupled with the CMA-GFS ADM through the adjoint of the interface programs (ad_black_carbon and ad_bc_driver). The adjoint of BC transport processes is also the same as that for the water-matter variables in CMA-GFS ADM, using the adjoint of QMSL. In this way, we got the CMA-GFS-AERO ADM. The structure of CMA-GFS-AERO ADM is shown in Fig. S3.~~

3.3 CMA-GFS-AERO 4D-Var

On the basis of the CMA-GFS-AERO ~~CCMM~~ forward model and its TLM and ADM, we further constructed the CMA-GFS-AERO 4D-Var by ~~adding the control variable of BC into~~adding BC as a control variable into the incremental analysis scheme introduced in Section 2.2. We also provided a detailed introduction to the BC observation and errors, the BC observation operator, and the background error covariance for BC.

3.3.1 BC mass concentration as control variable

The establishment of a strongly coupled aerosol-~~chemistry~~ meteorology 4D-Var system based on the CMA-GFS 4D-Var requires the addition of ~~atmospheric chemistry~~ aerosol analysis. Although the six variables for the mass mixing ratio of BC (ψ_{bc}^n~~ψ_{bc}~~) have been used in the CMA-GFS-AERO forward model, they can constitute a heavy burden for the analysis if they are all included in the control vector. The reasons for this, as mentioned by Benedetti et al. (2009), mainly include: (1) background error statistics would have to be generated for all variables separately, (2) the control vector would be significantly larger in size, which would consequently increase the cost of the iterative minimization, and most importantly, (3) the BC analysis would be under constrained since the surface observations of BC are mass concentrations (unit: μg/m^3), which do not distinguish between size bins, resulting in one observation of BC mass concentration being used to constrain six BC variables. To address these issues, the BC mass concentration is selected as the control variable, denoted as C_{bc} (unit: μg/m^3), and is added to the control vector ($x_u = (\psi, \chi_u, \pi_u, q)^T$, ψ is the stream function, χ_u is the unbalanced velocity potential, π_u is the unbalanced Exner pressure, and q is the specific humidity) of CMA-GFS 4D-Var. Thus, the control vector for the CMA-GFS-AERO 4D-Var is $x_u = (\psi, \chi_u, \pi_u, q, C_{bc})^T$, assuming that these five variables are independent of each other.

The conversion relationship between C_{bc} and ψ_{bc}^n~~ψ_{bc}~~ is

$$C_{bc} = \sum_{n=1}^{6} \psi_{bc}^n \psi_{bc}^{\ n} * \rho * 10^9, \quad (7)$$

where ρ is the atmospheric density, ~~n denotes the size bin of BC, and $\psi_{bc}^{\ n}$ represents the BC mass mixing ratio for size bin n~~. In order to obtain the BC initial field that can be used in the CMA-GFS-AERO model from the analysis field, it is also necessary to convert C_{bc} to $\psi_{bc}^n \psi_{bc}^{\ n}$. Firstly, ~~calculating~~ the distribution weights (ω^n) of each size bin of $\psi_{bc}^n \psi_{bc}^{\ n}$ in

the background field are calculated based on the entire three-dimensional domain, following the equation $\omega^n = \frac{\sum_1^N {\psi_{bc}}^n}{\sum_{n=1}^6 \left(\sum_1^N {\psi_{bc}}^n\right)}$, where N represents the number of three-dimensional grid points. Secondly, ~~calculating~~ the analysis increment of ψ_{bc}^n ~~ψ_{bc}~~^{n} ($\delta\psi_{bc}^n$ ~~$\delta\psi_{bc}$~~^{n}) is calculated based on the analysis increment of C_{bc} (δC_{bc}), following the equation

$$\delta\psi_{bc}^n \text{ } \delta\psi_{bc}^n = \omega^n * \frac{\delta C_{bc}}{\rho * 10^9}, \quad (8)$$

Finally, $\delta\psi_{bc}^n$ ~~$\delta\psi_{bc}$~~^{n} is interpolated and superimposed on ψ_{bc}^n ~~ψ_{bc}~~^{n} in the background field to obtain the initial field of BC. Similarly, in the minimization process of the inner loop of CMA-GFS-AERO 4D-Var, the conversion between the tangent linear variable of BC ($\delta\psi_{bc}^n$ ~~$\delta\psi_{bc}$~~) and the analysis increment of C_{bc} (δC_{bc}) is also calculated according to the derivative of Eq. (7) ($\delta C_{bc} = \sum_{n=1}^6 \delta\psi_{bc}^n$ ~~$\delta\psi_{bc}$~~$^n * \rho * 10^9$) and Eq. (8).

3.3.2 BC observation and errors

The BC observations used in the CMA-GFS-AERO 4D-Var system are the BC surface concentrations obtained from the China Atmospheric Monitoring Network (CAWNET), which was established by the CMA and has been monitoring the BC surface mass concentration in China since 2006 (Xu et al., 2020). The BC observation data were collected from 32 stations (Guo et al., 2020), including 11 urban, 17 rural and 4 remote stations. ~~and the~~ The distribution of these stations is shown in Fig. S24. The monitoring of BC in CAWNET was conducted using an Aethalometer, AE31, which is one of the models produced by Magee Scientific (USA, https://www.aerosolmageesci.com). The AE31 determines mass concentration of BC particles collected from air samples, flowing through a quartz filter. The instrument measures the transmission through the filter over a wide spectrum of wavelengths from 370 nm to 950 nm. Light at the selected wavelength is transmitted through control and sample filters, and the attenuation change in the filter is then translated into the BC mass concentration. In this study, we used the BC concentration measured at the recommended wavelength of 880 nm~~The BC observation instrument of CAWNET is the AE31 BC meter produced by Magee, USA, which uses continuous optical grayscale measurement method to calculate BC concentration in real time (Gong et al., 2019). The BC concentrations adopted here are hourly averages. They have undergone strict quality control before use and several invalid sites have been eliminated.~~ The AE31 measures BC concentrations every 5 minutes. We performed quality control on the original data and obtained the hourly average values, which were used in the BC assimilation experiments. The quality control procedures are as follows:

(1) Eliminating abnormal values. During the calculation of hourly averages from the 5-minute sampled data, any BC concentration values that differ significantly from the hourly average (i.e., those where the absolute difference exceeds three times the standard deviation) are considered abnormal and discarded. Additionally, any bad data flagged by the instrument's monitoring system are also removed.

(2) Filling in missing values. If more than one-third of the data for a given hour is missing, or if there are more than three consecutive missing values, the entire hour's data is discarded. For other cases, linear interpolation is applied to

fill in the missing values.

The observation error covariance matrix $\mathbf{R}$ in Eq. (1) contains both measurement and representativeness errors. Following the formula described by Chen et al. (2019), which is an improvement on the method proposed by Pagowski et al. (2010) and Schwartz et al. (2012), we calculated the measurement error ε_0. The formula is expressed as

$$\varepsilon_0 = 1.0 + 0.0075 \times O_{bc}, \quad (9)$$

where O_{bc} denotes the observed BC concentrations (unit: μg/m^3).

Representativeness errors reflect the inaccuracies in the forecast forward model and in the interpolation from the model grid to the observation location. We used the representativeness error (ε_r) expression defined by Elbern et al. (2007) as follow

$$\varepsilon_r = \gamma\varepsilon_0\sqrt{\frac{\Delta x}{L}}, \quad (10)$$

where γ is an adjustable parameter scaling ε_0 ($\gamma = 0.5$ was used here), Δx is the grid spacing (100 km in this work), and L is the radius of influence of a BC observation. According to Elbern et al. (2007), L was set to 2 km, 10 km, and 20 km for urban, rural, and remote stations, respectively~~(set to 10 km here)~~. The total BC observation error (ε_{bc}) was defined as

$$\varepsilon_{bc} = \sqrt{{\varepsilon_0}^2 + {\varepsilon_r}^2}, \quad (11)$$

which constituted the diagonal elements in the $\mathbf{R}$ matrix.

3.3.3 BC observation operator

The observation operator in the CMA-GFS-AERO 4D-Var system performs two basic tasks: (1) transforming model state variables into observed physical quantities, and (2) interpolating the background field (or analysis field) to the location of the observation. The transformation of the physical quantities is related to the type of observations, and the spatial interpolation operator consists of both horizontal and vertical interpolation. Since the CMA-GFS-AERO 4D-Var system adopts the Charney-Philips staggered grid~~variable staggering~~ in the vertical direction and the Arakawa-C grid in the horizontal direction, the observation operator must account for the staggered locations of different physical variables. To minimize errors introduced by variable transformations and spatial interpolation, appropriate handling of horizontal staggering and vertical layer transitions is required~~in the physical transformation of the observation operator, point jumps in the horizontal direction and layer jumps in the vertical direction should be performed according to the location of each element to reduce the errors introduced by variable transformation and spatial interpolation~~. The steps to construct the BC observation operator are as follows:

(1) Based on Eq. (7), the BC mass mixing ratios (ψ_{bc}^n~~ψ_{bc}~~) of six size bins are ~~accumulated~~summed and converted into the mass concentrations (C_{bc}), which are further interpolated to the observation locations by the horizontal bilinear interpolation to obtain the equivalent BC concentrations that are consistent with the units of the observations.

(2) According to the heights of BC surface observations, the corresponding vertical interpolation schemes are selected to

obtain the equivalent BC observations. If the height of BC surface observation is greater than the height of the first model layer, the cubic spline interpolation is used to process the BC concentration interpolation. If the observation height is less than the height of the first model layer~~,~~ and the difference between the two heights is less than 300 meters, the BC concentration at the first model layer is regarded as the equivalent BC observation~~;~~. ~~while~~However, if the difference between the two heights is greater than or equal to 300 meters, the data from that site is discarded.

3.3.4 Background error covariance for BC

The variable fields involved in variational assimilation are all three-dimensional, and it is challenging to directly deal with the correlations of these three-dimensional fields due to their high dimensionality. Therefore, in the CMA-GFS 4D-Var assimilation system, a simplification is made by assuming that the correlation coefficient can be expressed as the product of the vertical correlation coefficient and the horizontal correlation coefficient (Zhang et al., 2019). ~~And t~~The horizontal correlation is calculated using the spectral filtering method, while the vertical correlation is calculated through EOF decomposition (Zhang et al., 2019).

In the CMA-GFS-AERO 4D-Var system, the background error covariance for the control variable BC adopts a modeled structure. The background error variance varies with height as shown in Fig. 1a. The vertical correlation model of the background error is derived through a combination of theoretical considerations (Bergman, 1979) and experimental tuning, with particular reference to the methodology used for humidity in the CMA-GFS 4D-Var system. It is expressed as

$$R(z_i, z_j) = \frac{1}{1+k_z(z_i-z_j)^2}\ , \tag{12}$$

where z_i and z_j are the model terrain heights of level i and j, respectively. $k_z = \frac{g^2}{(R_d R T_0)^2} k_p$, g denotes the gravitational acceleration, R_d~~R~~ represents the gas constant for dry atmospheric air~~-~~, T_0 is the standard temperature (273.15 K), and k_p is the constant coefficient (Bergman, 1979). ~~taken as~~ Following the value of k_p used for the control variable of humidity in the CMA-GFS 4D-Var system, we set k_p to 10 ~~here~~ for the control variable BC. Figure 1b depicts the distribution of the vertical correlation coefficients of the background error of the 1st, 10th, and 20th layers with other layers.

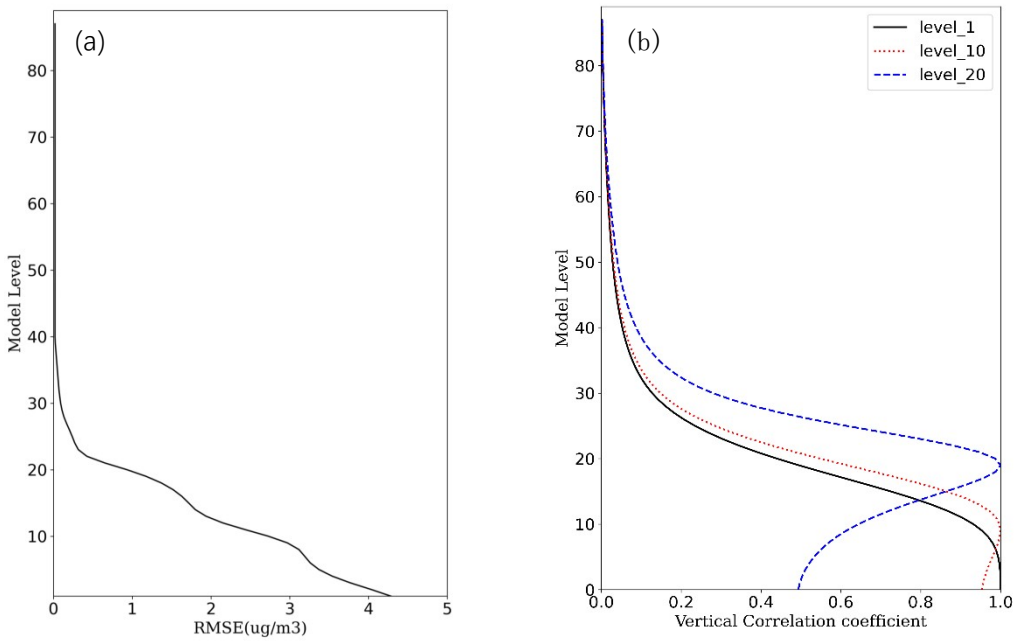

Figure 1: (a) Vertical profile of background error variance for BC, ~~Background error and~~ (b) vertical correlation coefficients of background error between the 1st, 10th, and 20th layers with other layers for BC.

The horizontal correlation of the background error for the control variable BC is calculated by the second-order auto-regressive (SOAR) correlation function, which is commonly used in operational data assimilation systems (Ballard et al., 2016), expressed as

$$r_{i,j} = \left(1 + \frac{d_{i,j}}{L}\right) \exp\left(-\frac{d_{i,j}}{L}\right), \quad (13)$$

where $d_{i,j}$ is the arc length of the great circle between two points i and j, L is the characteristic horizontal length scale~~, and t~~The length scale for the control variable BC varies with height in the model, following the way the length scale of the humidity variable varies with height in the CMA-GFS 4D-Var system~~is referenced to the relationship between the length scale of humidity and the height in CMA-GFS 4D-Var~~, which is shown in Table 1.

Table 1: Characteristic horizontal length scales of the background error.

Height (km)	length scale (km)
0.50	165
1.43	172
5.56	175
10.5	209
16.3	234
23.9	234

3.3.5 Flow-dependent background error covariance in CMA-GFS-AERO 4D-Var

In the strongly coupled aerosol-meteorology assimilation system, interactions between the atmospheric variables and BC allow BC observations to influence the analysis increment of atmospheric variables and vice versa. The incremental 4D-Var algorithm implicitly evolves the background error covariances (**B**) throughout the assimilation window according to the TL model dynamics. This process modifies prior background error variance estimates and induces non-zero correlations between model variables (Smith et al., 2015). By utilizing the fully coupled TLM and ADM in the inner loops of the strongly coupled assimilation system, cross-covariance information between BC and atmospheric variables is generated. This enables observations of one variable to produce analysis increments in the other, leading to more consistent analyses.

Specifically, if the BC observation is assumed to take place at the initial of the assimilation window, the 4D-Var assimilation is equivalent to the 3D-Var assimilation. Since the BC variable is assumed to be uncorrelated with the atmospheric variables in the static **B**, and there is no direct relationship between the BC observation operator and the atmospheric variables, the BC observation does not lead to the generation of the analysis increments of atmospheric variables. In this case, the merits of a coupled data assimilation system cannot be fully manifested by only assimilating a BC observation at the beginning of the window. If the BC observation is assumed to take place at the middle and the end of the assimilation window, **B** evolves within the assimilation time window through the TLM $\mathbf{M}_{0\to i}$, obtaining the implicit background error covariance matrix $\mathbf{M}_{0\to i}\mathbf{B}\mathbf{M}_{0\to i}^{T}$ that evolves with time. $\mathbf{M}_{0\to i}\mathbf{B}\mathbf{M}_{0\to i}^{T}$ includes the cross-covariances information of BC and atmospheric variables, and can realize the feedback of the BC observation to the atmospheric variables through the CMA-GFS-AERO ADM $\mathbf{M}_{0\to i}^{T}$, further producing analysis increments of atmospheric variables.

4 Model setup~~Results~~

~~**Model setup**~~

In this work, the horizontal resolution of the CMA-GFS-AERO ~~CCMM~~ forward model in the outer loop was set to 0.25°, with an integration step of 300 s, and the horizontal resolution of the CMA-GFS-AERO TLM and ADM in the inner loop was 1.0°, with an integration step of 900 s. The model has 87 vertical layers, with the top being approximately 0.1 hPa (Fig. S1). Referring to the running scheme of the CMA-GFS 4D-Var system described in Section 2.2, the CMA-GFS-AERO 4D-Var system also adopts the same 6-h cycling schedule and assimilation windows~~a 6-h cycle and is performed four times a day, with assimilation windows of 0300 UTC-0900 UTC, 0900 UTC-1500 UTC, 1500 UTC-2100 UTC and 2100 UTC-0300 UTC~~. The forecast of the CMA-GFS-AERO model started at 0300 UTC on October 1, 2016, and was restarted every 6 h. The meteorological initial fields for each 6-h cycle were obtained from the operational CMA-GFS analysis. The BC field

was initialized with null concentrations at 0300 UTC on October 1, 2016. From the second forecast cycle onward, the initial conditions of BC were derived from the BC field at the end of the previous 6-h forecast, allowing the BC field to be cycled~~was restarted every 6 h from operational CMA-GFS analysis, with BC field initialized from null concentrations at 0300 UTC on October 1, 2016. The BC field at the end of a given 6 h forecast was passed as initial conditions to the next 6 h forecast~~. ~~And t~~The first 9 days were used as the spin-up time to establish a realistic BC distribution. The maximum minimization iteration number in the inner loop was set to 50, while the outer loop was performed only once. This setting is consistent with the operational configuration of the CMA-GFS 4D-Var system and has been found sufficient for achieving convergence in our experiments. The atmospheric observations used in this work are shown in Table S1.

Anthropogenic emission sources used in this study were from the Multi-resolution Emission Inventory for China (MEIC) (Li et al., 2017; Zheng et al., 2018), the Copernicus Atmosphere Monitoring Service global and regional emissions (CAMS) (Granier et al., 2019), and the global datasets of the Task Force Hemispheric Transport of Air Pollution (HTAP) (Janssens-Maenhout et al., 2015)~~ datasets at a global scale~~. These inventories include various gases (NO_x, CO, SO_2, NH_3, CH_4 and NMVOC) and particulates (OC, BC, $PM_{2.5}$ and PM_{10}), where PM_{10} refers to the inhalable particulate matter with an aerodynamic diameter of 10 micrometers or less. ~~which~~These data were processed into grid-point emission data applicable to the CUACE model through the EMIPS emission source processing system (Chen et al., 2023)~~-~~. To improve computational efficiency, they were further simplified into emission source data containing only BC as input to the CMA-GFS-AERO model.

At present, we have run the CMA-GFS-AERO 4D-Var system for three months from October 1, 2016. This section mainly shows the experiment results of random time in these three months to present the rationality and stability of the system. The detailed results analysis of the batch test of the system will be further elaborated in part 2 of this paper.

5 Results

5.1 Validation of CMA-GFS-AERO TLM and ADM

Validation of the tangent linear and adjoint models is an important part of introducing a new modeling component, such as the AERO-BC module~~ an important part of introducing an adjoint model~~. Considering that CMA-GFS TLM and ADM have been validated and documented in Liu et al. (2017, 2023) and Zhang et al. (2019), here we mainly present the validation of tangent linear and adjoint of the newly developed AERO-BC module.

The correctness of the AERO-BC TL can be verified by checking whether the following equation is satisfied (Mahfouf and Rabier, 2000; Liu et al., 2017; Tian and Zou, 2020):

$$\Phi(\alpha) = \frac{\|\boldsymbol{F}(C+\alpha\cdot\delta C)-\boldsymbol{F}(C)\|}{\|\mathbf{F}(\alpha\cdot\delta C)\|} = 1 + O(\alpha), \quad (14)$$

where $\|.\|$ denotes the norm of the vector, α is the scale factor of initial perturbations with the range from 1.0 to 10^{-14}. As

the scale factor α becomes smaller and smaller, the function $\Phi(\alpha)$ is expected to approach unity in an approximately linear manner.~~way~~.

We firstly verified all submodules in the AERO-BC TL, finding that the tangent linear approximation of each submodule was correct. Subsequently, we conducted a set of six experiments with the integration time from 1 to 6 h to verify the correctness of the full AERO-BC TL. The background field and analysis increment generated by the CMA-GFS-AERO 4D-Var system were used as the basic-state initial field and the perturbation initial field of the CMA-GFS-AERO TLM for 6-hour forecasting. The atmospheric and BC state variables C and their perturbations δC of these six time periods were used as inputs of the AERO-BC and its TL, and the tangent linear approximation of the output variable (the perturbation of the mass mixing ratio of BC, $\delta\psi_{bc}^{n}$~~$\delta\psi_{be}$~~) of the AERO-BC TL is tested using Eq. (14).

Figure 2 shows the results of the six correctness experiments. As expected, in each verification experiment, as the scale factor α becomes smaller and smaller for certain ranges of α values, the values of $\Phi(\alpha)$ gradually get closer and closer to unity. When α is too small (such as 10^{-12}), the accuracies of the $\Phi(\alpha)$ values start to be affected by the machine round-off errors and drift away from unity. This indicates that the tangent linear approximation of the AERO-BC TL is correct.

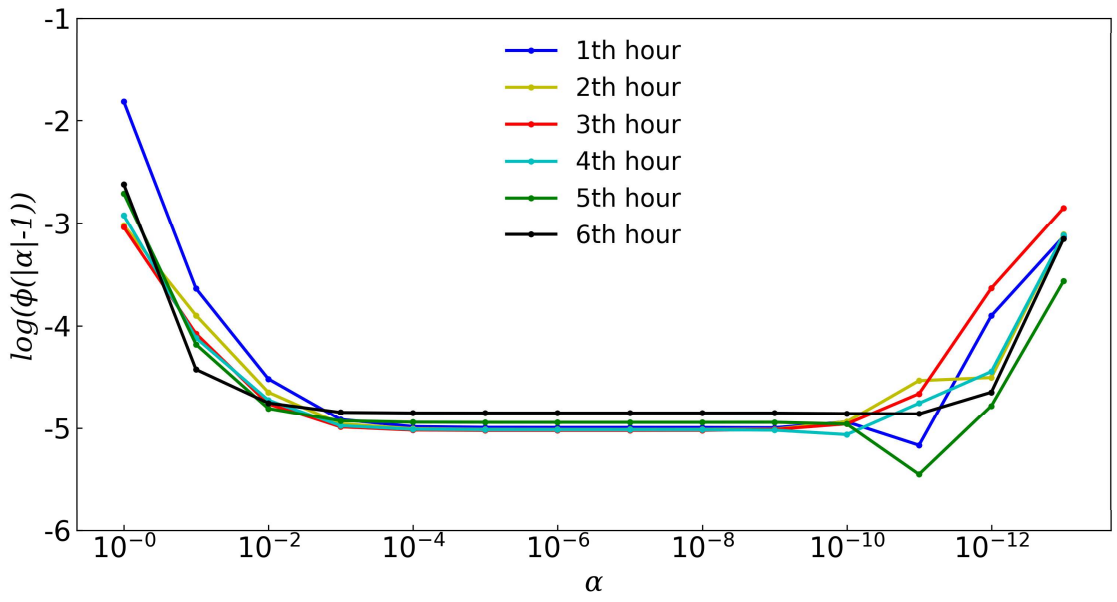

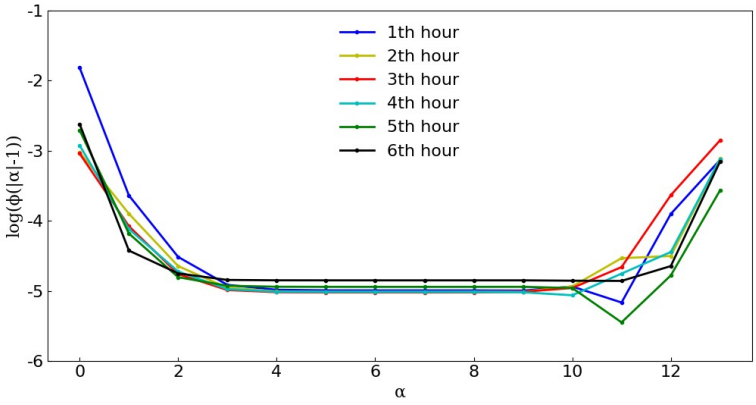

Figure 2: Variations in the function $|\Phi(\alpha)-1|$ for the correctness check of the AERO-BC TL for the 6-h forecast length, where α is the scale factor of initial perturbations.

We further diagnosed the impact of linearized physical processes on the forecast effectiveness of CMA-GFS-AERO TLM. Generally, the diagnostic method is to calculate the relative error (r) between the tangent linear perturbation forecast $\mathbf{M}(\delta x)$ and the nonlinear perturbation forecast $\Delta\boldsymbol{M}(\delta x)$ (Mahfouf, 1999; Liu et al., 2019; Zhang et al., 2019), which can be expressed as

$$r = \frac{|\mathbf{M}(\delta x) - \Delta\boldsymbol{M}(\delta x)|}{\Delta\boldsymbol{M}(\delta x)}. \quad (15)$$

The nonlinear perturbation forecast $\Delta\boldsymbol{M}(\delta x)$ is the difference between the NLM forecasts from two different initial conditions: the analysis ~~filed~~field x_a and the background ~~filed~~field x_b, that is $\Delta\boldsymbol{M}(\delta x) = \boldsymbol{M}(x_a) - \boldsymbol{M}(x_b)$. And the tangent linear perturbation forecast $\mathbf{M}(\delta x)$ is integrated using the analysis increment δx ($\delta x = x_a - x_b$) as the initial perturbation field. r needs to be calculated for each model variable at each grid.

The forecast period for this experiment was 6 h starting from 0300 UTC on October 25, 2016 (randomly selected time). For the nonlinear perturbation test, which includes the full physical processes, the two initial conditions were the analysis ~~filed~~field x_a and the background ~~filed~~field x_b generated by the CMA-GFS-AERO 4D-Var system at 0300 UTC on October 25, 2016. For the tangent linear perturbation test, the initial condition was the analysis increment δx ($\delta x = x_a - x_b$) at 0300 UTC on October 25, 2016. The model trajectory required for the tangent linear perturbation forecast was calculated by the CMA-GFS-AERO NLM including the full physical process with the background field x_b as the initial field. The nonlinear and tangent linear models were performed at the same resolution of 1.0°, and the analysis field x_a and the background field x_b were interpolated from 0.25° to 1.0° based on the 3D interpolation method (Huo et al., 2022).

Figure 3 depicts the results of the nonlinear perturbation forecast and the tangent linear perturbation forecast. Figure 3a-b show the differences in vertically accumulated and latitudinally averaged BC mass concentration (unit: μg/m^3) after 6-h integration of the CMA-GFS-AERO NLM with two initial conditions of x_a and x_b, respectively, and Fig. 3c-d present the vertically accumulated and latitudinally averaged BC mass concentration perturbations after 6-h integration of

CMA-GFS-AERO TLM with the initial condition of δx ($\delta x = x_a - x_b$), respectively. It can be seen that after 6-h forecast, the distribution of the results of CMA-GFS-AERO NLM and TLM, both horizontally and vertically, are very similar with only minor differences. This indicates that CMA-GFS-AERO TLM shows good performance in tangent linear approximation for BC.

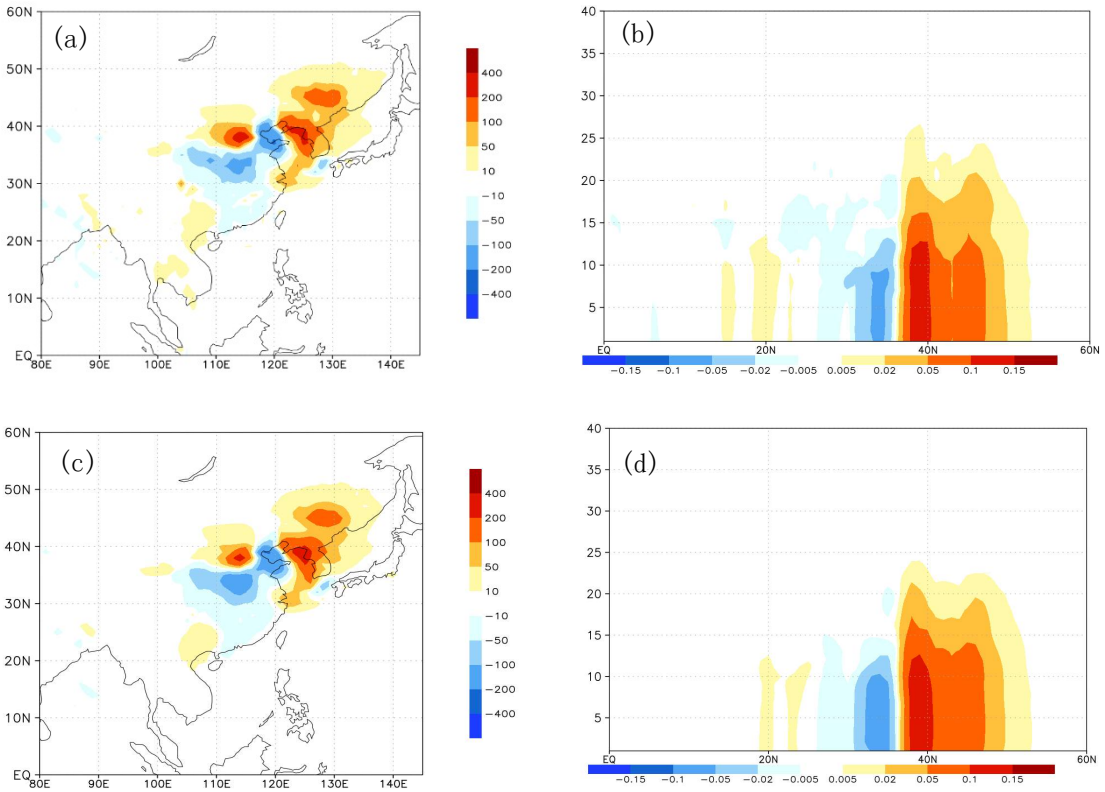

Figure 3: Differences in (a) vertically accumulated and (b) latitudinally averaged BC mass concentration (unit: μg/m^3) after 6-h integration of the CMA-GFS-AERO NLM with ~~two~~ initial conditions ~~of~~ x_a and x_b, and perturbations in~~of~~ (c) vertically accumulated and (d) latitudinally averaged BC mass concentration after 6-h integration of CMA-GFS-AERO TLM with the initial condition ~~of~~ δx ($\delta x = x_a - x_b$).

The vertical distribution of the globally averaged relative error between the perturbation forecasts of CMA-GFS-AERO TLM and NLM, which was calculated according to Eq. (15), is shown in Fig. 4. It can be seen that below the 20th model layer, the tangent linear approximation for BC is better than that for wind field, potential temperature, and specific humidity. Although the tangent linear approximation for BC is slightly worse above the 20th model layer, it is still far better than that for specific humidity. It's worth noting that the BC concentration above the 20th model level is quite low (Fig. 3b), so the impact of the tangent linear approximation is minimal. This phenomenon indicates that, in comparison to variables such as potential temperature and specific humidity, ~~as a coupled variable similar to a physical process variable~~ in the CMA-GFS-AERO model, the tangent linear approximation for BC is quite effective, making it well-suited for constructing a 4D-Var system.

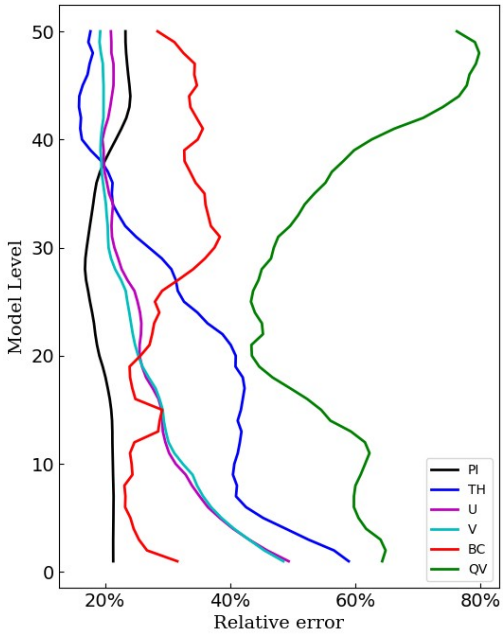

Figure 4: The vertical distribution of the globally averaged relative error between the perturbation forecasts of~~in~~ the CMA-GFS-AERO TLM ~~with simple physics with respect to the~~ and NLM ~~with full physics~~ at the resolution of 1.0°. (black line: non-dimensional pressure, blue line: potential temperature, red line: BC, magenta line: u-wind, cyan line: v-wind; green line: specific humidity).

The correctness of the AERO-BC adjoint can be verified by checking whether the following equation is satisfied (Mahfouf and Rabier, 2000; Liu et al., 2017; Tian and Zou, 2020)

$$\langle \mathbf{F}(\delta C), \mathbf{F}(\delta C) \rangle = \langle \delta C, \mathbf{F}^T\big(\mathbf{F}(\delta C)\big) \rangle, \quad (16)$$

where $\langle , \rangle$ denotes the inner product. Using δC as the input of the AERO-BC TL, the output of the AERO-BC TL $\mathbf{F}(\delta C)$ can be obtained and the left-hand side (LHS) of Eq. (16) can be calculated. Then, taking $\mathbf{F}(\delta C)$ as the input of the AERO-BC adjoint, we can get its output $\mathbf{F}^T\big(\mathbf{F}(\delta C)\big)$ and calculate the right-hand side (RHS). If the AERO-BC adjoint is developed correctly, the LHS and RHS of Eq. (16) is expected to agree with the machine accuracy of the data type declared in the program, which is double precision in the AERO-BC.

Following Eq. (16), we ~~set~~ conducted five experiments with the integration time equal to 1, 6, 12, 24, and 36 steps with the time step of 900 s. Considering the mass mixing ratio of BC ($\psi_{bc}^n \psi_{b\epsilon}$) as an example, for each experiment, the atmospheric variables and $\psi_{bc}^n \psi_{b\epsilon}$ perturbations in the analysis increment generated by the CMA-GFS-AERO 4D-Var system was used as the input of the AERO-BC TL. We run the tangent linear codes once to obtain the value of the tangent linear output, and calculated the LHS of Eq. (16). Then, taken the tangent linear output as input, the AERO-BC adjoint codes was run once to

obtain the sensitivity value, which further was used to calculated the RHS of Eq. (16) with the $\psi_{bc}^{n}\psi_{bc}$ perturbation. The validation results are presented in Table 2. The resulting LHS and RHS from the five tests agree with the precision of machine accuracies, indicating the correctness of the AERO-BC adjoint model.

Table 2: Correctness check results of the newly developed AERO-BC adjoint model when it is integrated for 1, 6, 12, 24, and 36 steps.

Step	LHS	RHS	(LHS-RHS)/LHS
1	6. 048801009887637E-015	6. 048801009887634E-015	5.2166431260112900E-16
6	5. 661147803064362E-015	5. 661147803064381E-015	3.3443150371477720E-15
12	5. 608184349558140E-015	5. 608184349558160E-015	3.6572234893387934E-15
24	5. 694921201673081E-015	5. 694921201673082E-015	1.3852007381406021E-16
36	5. 845344664075793E-015	5. 845344664075791E-015	2.6991082666833257E-16

LHS: left-hand side of Eq. (16); RHS: right-hand side of Eq. (16).

5.2 Single point observation ideal experiment

In order to evaluate the rationality of the CMA-GFS-AERO 4D-Var system, we performed set the single point observation ideal experiment for BC. The experiment period was 6 h starting from 0300 UTC on November 24, 2016 (randomly selected time), and the forecast field of the CMA-GFS-AERO model at this time was selected as the background filedfield. During the assimilation process, no atmospheric observations were added. We adopted the BC surface observation at Nanjiao station (116.47°E, 39.8°N), which is located in Beijing, at 0300 UTC on November 24, 2016. The altitude of Nanjiao station is 31.3 meters, and the observed BC concentration is 10.0 μg/m³. Figure S5 shows the location of the BC observation and the wind field at 925hPa, which moves from northwest to southeast. The BC observation was set placed at 0300, 0600, and 0900 UTC, respectively, corresponding to the initial, the middle, and the end of the assimilation time window.

Theoretically, the analysis increment at the initial time for 4D-Var assimilation is $\delta x = \mathbf{B}\sum_{i=0}^{n}\mathbf{M}_{0\to i}^{T}\mathrm{H}_i^{T}\left(\mathrm{H}_i\mathbf{M}_{0\to i}\mathbf{B}\mathbf{M}_{0\to i}^{T}\mathrm{H}_i^{T}+\mathbf{R}_i\right)^{-1}(-d_i)$. If we only assimilate the observation at time t_i, the analysis increment at the observation time is $\mathbf{M}_{0\to i}\delta x = \mathbf{M}_{0\to i}\mathbf{B}\mathbf{M}_{0\to i}^{T}\mathbf{H}_i^{T}\left(\mathbf{H}_i\mathbf{M}_{0\to i}\mathbf{B}\mathbf{M}_{0\to i}^{T}\mathbf{H}_i^{T}+\mathbf{R}_i\right)^{-1}(-d_i)$. When assimilating the single point observation, $\left(\mathbf{H}_i\mathbf{M}_{0\to i}\mathbf{B}\mathbf{M}_{0\to i}^{T}\mathbf{H}_i^{T}+\mathbf{R}_i\right)^{-1}(-d_i)$ is a vector with only one factor. If the observation position and the analysis grid coincide, the spatial interpolation in the observation operator can be ignored. Thus, the analysis increment at the observation time can reflect the structure of the background field error covariance $\mathbf{M}_{0\to i}\mathbf{B}\mathbf{M}_{0\to i}^{T}$ at the observation time. Figure 5 shows the analysis increments of BC at the first model layer at the observation times, with the BC observation set placed at 0300, 0600, and 0900 UTC, respectively. When the BC observation is placed set at 0300 UTC (the observation innovation increment ($d_i =$

$\boldsymbol{H}_i\boldsymbol{M}_{0\to i}(x_b) - y_i$) is -1.2 μg/m^3 at 0300 UTC), the 4D-Var assimilation is equivalent to the 3D-Var assimilation, and the horizontal distribution of the BC analysis increment is determined by the static background ~~field~~ error covariance model **B**. Since the CMA-GFS-AERO 4D-Var system uses a homogeneous second-order autoregressive spatial correlation model, the BC analysis increment at 0300 UTC (Fig. 5a) is essentially isotropic, and only the background ~~field~~ error covariance, which varies with latitude, causes the analysis increments to differ somewhat in the north-south direction. When the BC observation is placed ~~set~~ at 0600 UTC (the observation innovation ~~increment~~ is -9.5 μg/m^3 at 0600 UTC) and 0900 UTC (the observation innovation ~~increment~~ is -9.0 μg/m^3 at 0900 UTC), the BC analysis increments show anisotropic characteristics (Fig. 5b-c), which is consistent with the movement of the wind at 925hPa (Fig. S3~~5~~), indicating that the background ~~field~~ error covariance varies with the weather situation. Meanwhile, it can also be seen that the values of the BC analysis increments at 0600 and 0900 UTC are much larger than those at 0300 UTC. This is because the BC observation innovation ~~increments~~ at 0600 and 0900 UTC are greater than those at 0300 UTC.

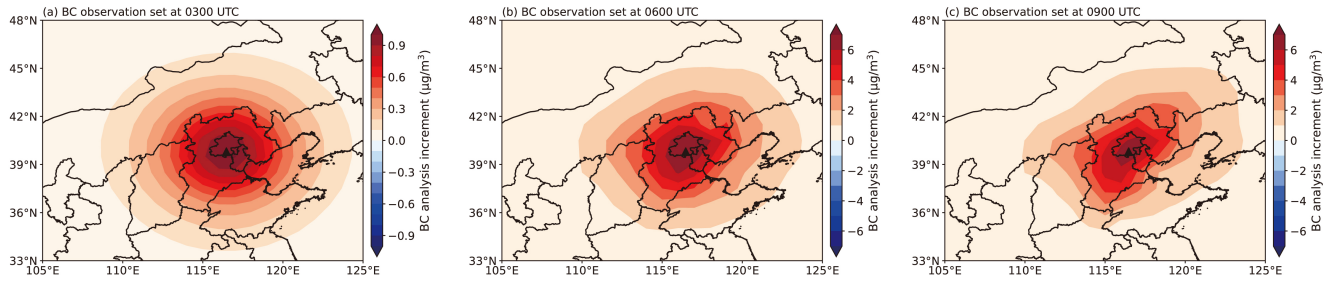

Figure 5: The analysis increments of BC at the first model level at the observation times, with the BC observation ~~set~~ placed at (a) the initial of the assimilation time window, 0300 UTC; (b) the middle of the assimilation window, 0600 UTC; (c) the end of the assimilation time window, 0900 UTC. The black triangle represents the ideal observation location (116.47°E, 39.8°N).

Figure 6 presents the evolved analysis increments of BC at the first model level at the end of the assimilation time window (0900 UTC) obtained by CMA-GFS-AERO TLM, with the BC observation ~~set~~ placed at 0300 and 0600 UTC, respectively. For the case where the BC observation is placed at 0300 UTC, the initial analysis increment at 0300 UTC (Fig. 5a) exhibits an isotropic structure due to the static B. In contrast, the propagated analysis increment at the end of the assimilation time window (0900 UTC, Fig. 6a) exhibits an anisotropic structure under the influence of the flow-dependent $M_{0\to i}BM_{0\to i}^{T}$. Similarly, when the BC observation is placed at 0600 UTC, both the initial analysis increment at 0600 UTC (Fig. 5b) and the propagated analysis increment at 0900 UTC (Fig. 6b) exhibit an anisotropic structure. In addition, the horizontal distribution structure of the BC analysis increments in Fig. 6a and Fig. 6b closely resembles that of the analysis increments at the observation time of 0900 UTC (Fig. 5c). This indicates the significant impact of flow-dependent dynamics on the evolution of the analysis increments. ~~The BC analysis increments show a more similar horizontal distribution structure relative to the analysis increments at the observation time of 0900 UTC (Fig. 5c). This is because no~~ No matter what time the observation is

~~set~~ placed at, the spatial propagation of the observation information is effectively achieved through the model integration. In this idealized single-point observation experiment, the propagation of BC increments is primarily dominated by advection due to the limited observational constraint. When more comprehensive observations are assimilated, advection remains a key factor, but its dominance is less pronounced as other processes also influence the adjustment of BC distributions (see Section 5.3).

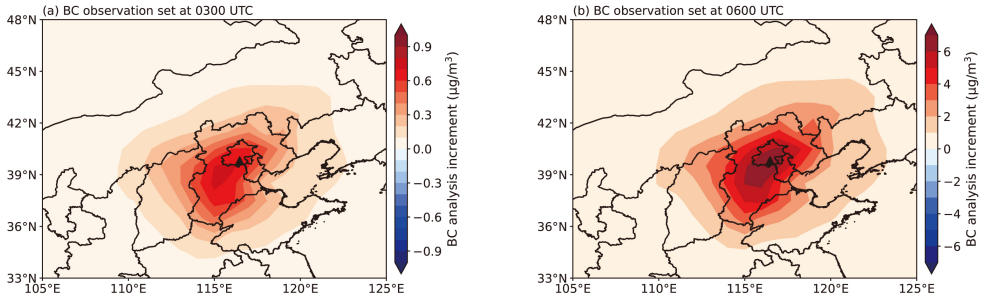

Figure 6: The analysis increments of BC at the first model level at the end of the assimilation time window, 0900 UTC, with the BC observation ~~set~~ placed at (a) the initial of the assimilation window, 0300 UTC; (b) the middle of the assimilation window, 0600 UTC. The black triangle represents the ideal observation location (116.47°E, 39.8°N).

~~As mentioned above, when the BC observation is assumed to take place set at 0300 UTC, the 4D-Var assimilation is equivalent to the 3D-Var assimilation. Since the BC variable is assumed to be uncorrelated with the atmospheric variables in the static **B**, and there is no direct relationship between the BC observation operator and the atmospheric variables, the BC observation does not lead to the generation of the analysis increments of atmospheric variables. In this case, although the BC control variable is minimized together with the atmospheric variables in the CMA-GFS-AERO 4D-Var system, it still cannot be considered as the coupled assimilation in essence.~~ Figure 7 depicts the analysis increments of temperature at the first model level at the initial time of the assimilation time window (0300 UTC), with the BC observation ~~set~~ placed at 0600 and 0900 UTC, respectively. It can be seen that when the BC observation is ~~set~~ placed at 0600 and 0900 UTC, positive analysis increments of temperature are generated, with the value of about 0.02 K near the observation location. The mechanism behind the generation of these temperature increments is detailed in Section 3.3.5. ~~**B** evolves within the assimilation time window through the TLM $\mathbf{M}_{0\to i}$, obtaining the implicit background error covariance matrix $\mathbf{M}_{0\to i}\mathbf{B}\mathbf{M}_{0\to i}^{T}$ that evolves with time. $\mathbf{M}_{0\to i}\mathbf{B}\mathbf{M}_{0\to i}^{T}$ includes the error co-correlation information of BC and atmospheric variables, and can realize the feedback of the BC observation to the atmospheric variables through the CMA-GFS-AERO ADM $\mathbf{M}_{0\to i}^{T}$, further producing positive analysis increments of temperature, with the value of about 0.02 K near the observation location (Fig. 7).~~ This indicates that the temperature of the analysis field will increase due to the assimilation of the BC observation.

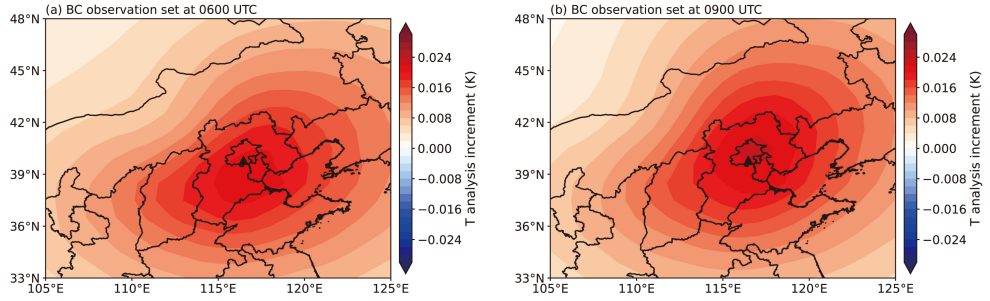

Figure 7: The analysis increments of temperature at the first model layer at the initial of the assimilation time window, 0300 UTC, with the BC observation ~~set~~ placed at (a) the middle of the assimilation window, 0600 UTC; (b) the end of the assimilation time window, 0900 UTC. The black triangle represents the ideal observation location (116.47°E, 39.8°N).

Figure 8 shows the analysis increments of pressure, east-west component of horizontal wind, and relative humidity at the first model level at the initial of the assimilation time window (0300 UTC), with the BC observation ~~set~~ placed at 0900 UTC. It is obvious that the single ~~point~~ BC observation assimilation produces a certain degree of analysis increments of pressure, east-west component of horizontal wind, and relative humidity in North China, which shows that the CMA-GFS-AERO 4D-Var coupled assimilation system can reflect the impact of BC assimilation on atmospheric increments. In ~~fact~~reality, ~~–~~ unlike the single observation experiment, the BC observation is distributed within the assimilation time window, rather than just at a fixed moment, thus, the advantages of the CMA-GFS-AERO 4D-Var strong coupling assimilation system can be fully utilized to explore the feedback ~~effect~~ of BC assimilation on atmospheric variables.

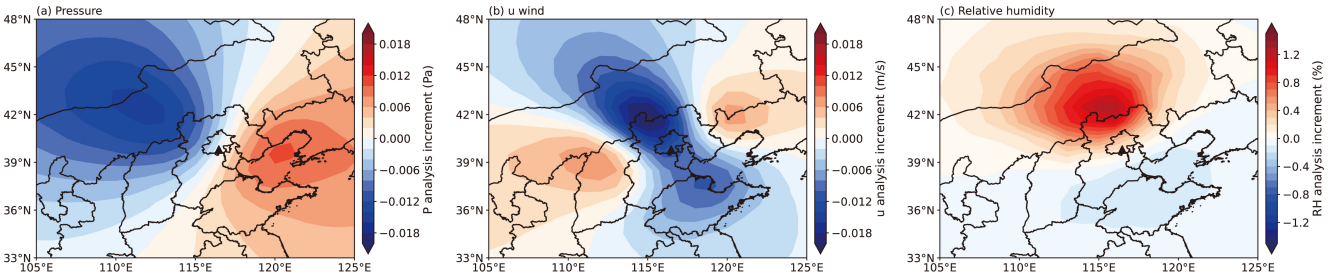

Figure 8: The analysis increments of (a) pressure, (b) east-west component of horizontal wind, and (c) relative humidity at the first model layer at the initial of the assimilation time window, 0300 UTC, with the BC observation ~~set~~placed at the end of the assimilation time window, 0900 UTC. The black triangle represents the ideal observation location (116.47°E, 39.8°N).

5.3 Case study on BC and atmosphere assimilation

On the basis of the single ~~point~~ observation ~~ideal~~ experiment, we further conducted ~~set~~ the full observation experiment for BC and atmospheric variables. The experiment period was also 6 h starting from 0300 UTC on November 24, 2016 (the same time as the experimental setup in Section 5.2~~4.3~~), and the forecast field of the CMA-GFS-AERO model at this time was selected as the background ~~filed~~field. We conducted a set of four experiments~~,~~ to investigate the impact of different BC

assimilation strategies on both BC and atmospheric variables. These experiments are listed in Table 1.~~and the observations assimilated in each experiment are shown in Table 3. It's worth noting that in EXP3, operational meteorological observations were assimilated first, followed by BC surface observations, and atmospheric variables and the BC variable were minimized separately. This is actually the weakly coupled assimilation. While in EXP4, BC surface observations and operational meteorological observations were assimilated simultaneously, and the BC variable and atmospheric variables were minimized together, which is the strongly coupled assimilation.~~ Different from the single~~-point~~ observation ~~ideal~~ experiment in Section 5.2~~4.3~~, in which the observations are placed at a fixed time, we assimilated all available BC observations with an hourly frequency within the assimilation time window in the full observation experiment. In the following analysis, we primarily compare the BC analysis increments obtained from DA_BC, DA_MET_then_BC, and DA_MET_BC_simult experiments, noting that the BC analysis increments from the DA_MET experiment are very small (figure omitted). Additionally, we compare the atmospheric analysis increments caused by BC assimilation in DA_BC, DA_MET_then_BC (DA_MET_then_BC-DA_MET), and DA_MET_BC_simult (DA_MET_BC_simult-DA_MET).

Table 3: Design of four assimilation experiments.

Experiments	Description
DA_BC	Assimilating only BC surface observations while excluding operational meteorological observations
DA_MET	Assimilating only operational meteorological observations while excluding BC surface observations
DA_MET_then_BC	First assimilating operational meteorological observations, then assimilating BC surface observations
DA_MET_BC_simult	Assimilating both operational meteorological and BC surface observations simultaneously

~~Experiments~~	~~Assimilated observations~~
~~EXP1~~	~~Only BC surface obs.~~
~~EXP2~~	~~Only operational meteorological obs.~~
~~EXP3~~	~~Operational meteorological obs. and BC surface obs., minimized separately~~
~~EXP4~~	~~Operational meteorological obs. and BC surface obs., minimized together~~

Figure 9 presents the analysis increments of BC at the first model layer from the DA_BC, DA_MET_then_BC, and

DA_MET_BC_simult experiments~~EXP1, EXP3, and EXP4~~. When only BC surface observations are assimilated (DA_BC~~EXP1~~), the BC analysis increment is mainly concentrated~~distributed~~ in North China and Eastern China, with a maximum value of about 6.0 μg/m^3 (Fig. 9a). When operational meteorological observations are assimilated first, followed by BC surface observations (DA_MET_then_BC), or when both operational meteorological and BC surface observations are assimilated simultaneously (DA_MET_BC_simult), the distribution and the value of BC analysis increments are nearly identical to those of DA_BC, with only minor differences (Fig. 9b-c). This indicates that the three BC assimilation strategies have similar assimilation effects on BC, further demonstrating that the assimilation of meteorological observations has a relatively small impact on BC analysis increments.~~When both operational meteorological observations and BC surface observations are assimilated (EXP3 and EXP4), regardless of whether the BC variable and atmospheric variables are minimized together, the distribution and the value of BC analysis increments are basically consistent with EXP1, with slight differences (Fig. 9b-c). This implies the slight impact of assimilation of meteorological observations on BC analysis increments, and also indicates the similar assimilation effects of the weakly coupled assimilation and the strongly coupled assimilation on BC.~~

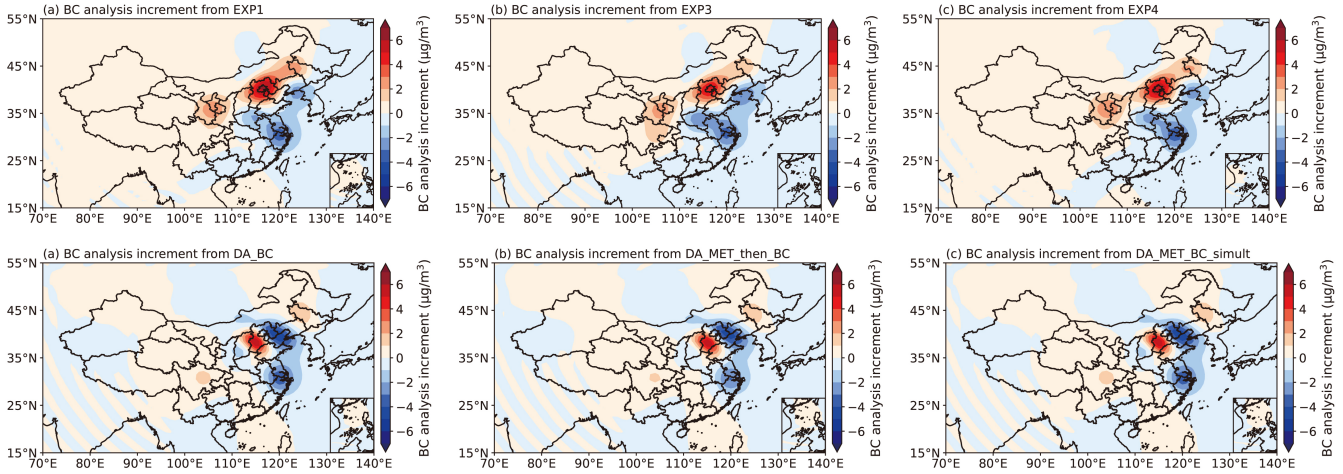

Figure 9: The analysis increments of BC at the first model layer from (a) DA_BC~~EXP1~~, (b) DA_MET_then_BC~~EXP3~~, and (c) DA_MET_BC_simult~~EXP4~~.

We further explored the impact of different BC assimilation strategies on analysis increments of atmospheric variables. Figure 10 shows the analysis increments of temperature, pressure, east-west component of horizontal wind, and relative humidity at the first model layer, resulting from BC assimilation in DA_BC, DA_MET_then_BC, and DA_MET_BC_simult. The increments in Fig. 10 are excluded the contributions from the assimilation of operational meteorological observations. Panels 10a, 10d, 10g, and 10j display the analysis increments of these variables from BC assimilation in DA_BC. Panels 10b, 10e, 10h, and 10k show the increments due to BC assimilation in DA_MET_then_BC, obtained by subtracting the atmospheric increments in DA_MET from DA_MET_then_BC (DA_MET_then_BC-DA_MET). Panels 10c, 10f, 10i, and

10l illustrate the increments caused by BC assimilation in DA_MET_BC_simult, obtained similarly by subtracting the increments in DA_MET from DA_MET_BC_simult (DA_MET_BC_simult - DA_MET).

~~We further explored the impact of assimilating BC surface observations on analysis increments of atmospheric variables. Figure 10a, 10d, 10g, and 10j present the analysis increments of temperature, pressure, east-west component of horizontal wind, and relative humidity, respectively, at the first model layer from EXP1, showing the impact of assimilating only BC surface observations on the analysis increments of atmospheric variables. Figure 10b, 10e, 10h, and 10k are the analysis increments of these four atmospheric variables at the first model layer from EXP3, presenting the impact of assimilating BC surface observations on the analysis increments of atmospheric variables in the weakly coupled assimilation. Figure 10c, 10f, 10i, and 10l depict the differences of analysis increments of these four atmospheric variables between EXP4 and EXP2 (EXP4 minus EXP2), reflecting the impact of assimilating BC surface observations on the analysis increments of atmospheric variables in the strongly coupled assimilation. It can be seen that when only BC surface observations are assimilated (EXP1), there are certain degrees of analysis increments of temperature (Fig. 10a), pressure (Fig. 10d), east-west component of horizontal wind (Fig. 10g), and relative humidity (Fig. 10j) distributed in North China and Eastern China, which is consistent with the distribution of BC analysis increments (Fig. 9). The value of the analysis increments of temperature, pressure, east-west component of horizontal wind, and relative humidity can reach about 0.1K (Fig. 10a), ± 0.04Pa (Fig. 10d), -0.14m/s (Fig. 10g), and 3.5% (Fig. 10j), respectively. When both operational meteorological observations and BC surface observations are assimilated in a weakly coupled manner (EXP3), the distributions and the values of the analysis increments of these four atmospheric variables (Fig. 10b, e, h, k) are basically consistent with those of EXP1. This indicates that the impact of the weakly coupled assimilation on the analysis increments of atmospheric variables is almost the same as the impact of assimilating only BC observations.~~

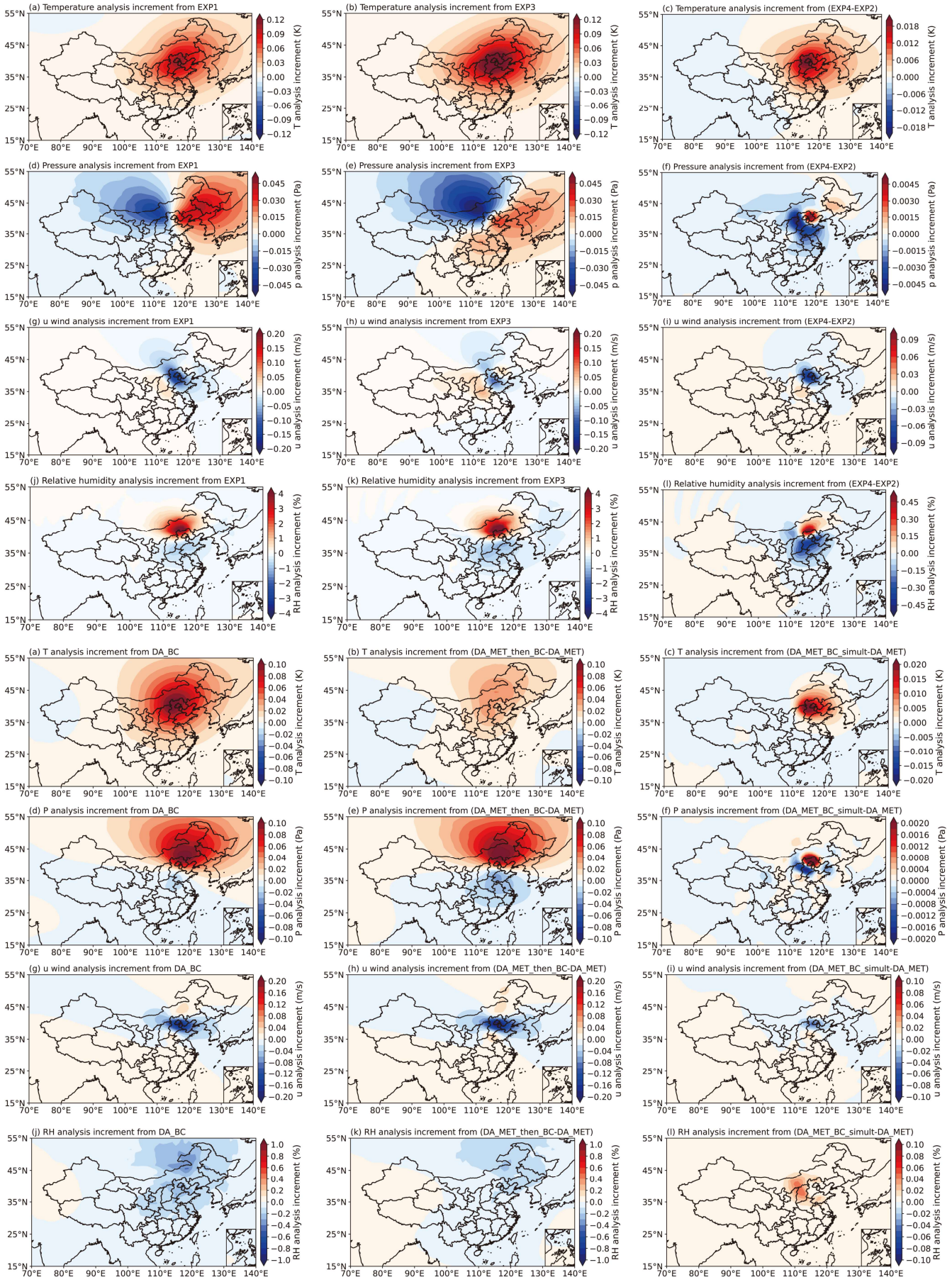

Figure 10: The analysis increments of (a, b, c) temperature, (d, e, f) pressure, (g, h, i) east-west component of horizontal wind, and (j, k, l) relative humidity at the first model layer caused by BC assimilation. (a, d, g, j) are analysis increments from ~~EXP1~~DA_BC, (b, e, h, k) are ~~analysis increments from EXP3~~ the differences in analysis increments between DA_MET_then_BC and DA_MET

(DA_MET_then_BC minus DA_MET), and (c, f, i, l) are the differences in analysis increments between DA_MET_BC_simult~~EXP4~~ and DA_MET~~EXP2~~ (DA_MET_BC_simult~~EXP4~~ minus DA_MET~~EXP2~~).

When only BC surface observations are assimilated (DA_BC), analysis increments of temperature (Fig. 10a), pressure (Fig. 10d), east-west component of horizontal wind (Fig. 10g), and relative humidity (Fig. 10j) are present in North China and Eastern China. The value of the analysis increments for temperature, pressure, east-west component of horizontal wind, and relative humidity reach approximately 0.1 K (Fig. 10a), 0.1 Pa (Fig. 10d), -0.2 m/s (Fig. 10g), and 0.8% (Fig. 10j), respectively. When operational meteorological observations are assimilated first, followed by BC surface observations (DA_MET_then_BC), the distributions and the values of the analysis increments of these four atmospheric variables due to BC assimilation (Fig. 10b, e, h, k) are basically consistent with those of DA_BC. This is because, although DA_MET_then_BC first assimilates operational meteorological observations and then BC surface observations, the BC assimilation step only incorporates BC observations, just like in DA_BC. Therefore, the analysis increments of atmospheric variables caused by BC observations in both DA_MET_then_BC and DA_BC are similar. Additionally, the values in each sub-image of the middle panel in Fig. 10 differ slightly from those on the left. These differences are attributed to the distinct basic-state values of the atmospheric variables used in the two experiments. In DA_BC, the basic-state values of the atmospheric variables used in the tangent linear and adjoint processes are derived from the atmospheric background field information without assimilating operational meteorological observations, while in DA_MET_then_BC, the basic-state values are based on the atmospheric analysis field information after assimilating the operational meteorological observations. The overall distribution and pattern of the analysis increments of temperature (Fig. 10c), pressure (Fig. 10f), and the east-west component of horizontal wind (Fig. 10i) caused by BC assimilation in DA_MET_BC_simult are consistent with those in DA_BC and DA_MET_then_BC. However, the increment values in DA_MET_BC_simult are smaller, with values reaching approximately 0.02 K (Fig. 10c), 0.002 Pa (Fig. 10f), and -0.05 m/s (Fig. 10i), respectively. The analysis increment of relative humidity (Fig. 10l) due to BC assimilation in DA_MET_BC_simult shows a small positive value distribution, whereas in DA_BC and DA_MET_then_BC, it exhibits a negative value distribution. The differences in analysis increments of the four atmospheric variables caused by BC assimilation between DA_MET_BC_simult and DA_BC/DA_MET_then_BC may be due to the fact that information fusion reduces the impact of individual observation. As mentioned above, DA_MET_then_BC is similar to DA_BC in that, in the process of BC assimilation, only BC surface observations are incorporated into the assimilation system. At this stage, the system relies solely on BC observations to correct the initial field. In the absence of atmospheric observations, BC observations play a dominant role, leading to larger analysis increments of atmospheric variables. In contrast, in DA_MET_BC_simult, both operational meteorological observations and BC surface observations are assimilated simultaneously. In this scenario, atmospheric observations provide more comprehensive or reliable information, which may reduce the dominant influence of the BC observations on the

analysis increments of atmospheric variables. As a result, a more balanced adjustment of atmospheric variables is achieved in DA_MET_BC_simult.

The preliminary results obtained from this set of four experiments indicate that different BC assimilation strategies have little impact on BC analysis increments but significantly affect the analysis increments of atmospheric variables. When only BC observations are assimilated, the influence of BC on atmospheric variables is more pronounced, whereas the simultaneous assimilation of meteorological observations moderates this influence. This suggests that in BC assimilation, meteorological observations can help constrain the uncertainty introduced by BC observations on atmospheric variables, thereby improving the reliability of the assimilation results. Moreover, these results demonstrate the successful implementation of the newly developed CMA-GFS-AERO 4D-Var system and highlight it as an effective approach for investigating the feedback of BC data assimilation on meteorological forecasts. In the future, we will conduct batch experiments using CMA-GFS-AERO 4D-Var to gain deeper insights into the role of BC assimilation in numerical weather prediction and further refine the system for broader applications.

~~From the differences between EXP4 and EXP2, it can be found that the distribution of the analysis increments of temperature (Fig. 10c), pressure (Fig. 10f), east-west component of horizontal wind (Fig. 10i), and relative humidity (Fig. 10l) are similar to those of EXP1 and EXP3. Although the distribution of the pressure analysis increments is not as extensive as those of EXP1 and EXP3, it also shows a pattern of negative values in the west of North China and positive values in the east of North China. It is worth noting that the values in each sub-image of the right panel in Fig. 10 are about an order of magnitude smaller than those on the left and the middle. This implies that when both operational meteorological observations and BC surface observations are assimilated in a strongly coupled manner (EXP4), the feedback on atmospheric analysis is constrained by the atmospheric observations, resulting in the analysis increments being much smaller than assimilating BC observations alone and the weakly coupled assimilation. Therefore, when considering the feedback effect of BC assimilation on atmospheric analysis, it is necessary to assimilate atmospheric observations and BC observations in a strongly coupled manner, otherwise the feedback effect may be amplified.~~

5.4 Computational performance of CMA-GFS-AERO 4D-Var

This section presents the computational performance of CMA-GFS-AERO 4D-Var from three aspects: (1) forward model, (2) TLM and ADM, and (3) 4D-Var system. We firstly evaluated the computational performance of a CMA-GFS-AERO simulation and compared it with that of the CMA-GFS simulation. Table 4 shows the computational costs for 6 h, 24 h, and 120 h integrations of CMA-GFS and CMA-GFS-AERO models. It can be seen that for 6 h, 24 h, and 120 h forecasts with the same integration time step (300 s), the same horizontal resolution of 0.25°, and the same number of CPU cores (1920 cores), the CMA-GFS-AERO simulations increase only about 10% of the computational time of the CMA-GFS simulations (As a reference, the microphysics process accounts for approximately 5% of the total computation time in CMA-GFS

simulations). This shows the high efficiency of CMA-GFS-AERO forward model ~~CCMM~~, which is an important factor in developing a strongly coupled ~~chemistry~~ aerosol-meteorology 4D-Var system.

Table 4: Computational costs (unit: s) for 6 h, 24 h, and 120 h integrations of CMA-GFS and CMA-GFS-AERO models.

Model/Integration time	6 h	24 h	120 h
CMA-GFS	111.5	366.6	1725.2
CMA-GFS-AERO	121.9	403.5	1930.5

Note: The CMA-GFS and CMA-GFS-AERO models are integrated with the same time step (300 s), the same horizontal resolution of 0.25°, and the same CPU cores (1920 cores).

Table 5 presents the computational costs for 12 h integrations of CMA-GFS TLM/ADM and CMA-GFS-AERO TLM/ADM, and Table 6 shows the computational costs for 6 h integrations of CMA-GFS 4D-Var and CMA-GFS-AERO 4D-Var. It is apparent that with an increasing number of CPU cores, the acceleration effects of CMA-GFS-AERO TLM, ADM, and 4D-Var are comparable to those of CMA-GFS TLM, ADM, and 4D-Var. When using 1440 CPU cores, the total time of CMA-GFS-AERO TLM, ADM, and 4D-Var are approximately 1.1 times, 1.2 times, and 1.4 times those of CMA-GFS TLM, ADM, and 4D-Var, respectively. This highlights the high efficiency and good scalability of CMA-GFS-AERO TLM, ADM, and 4D-Var, making the coupled aerosol-~~chemistry~~ meteorology 4D-Var system potentially suitable for operational application.

Table 5: Computational costs (unit: s) for 12 h integrations of CMA-GFS TLM/ADM and CMA-GFS-AERO TLM/ADM.

Model\CPU core	480	960	1440
CMA-GFS TLM	14.63	8.95	7.04
CMA-GFS ADM	19.25	11.14	8.07
CMA-GFS-AERO TLM	16.58	10.18	7.55
CMA-GFS-AERO ADM	22.92	12.96	9.31

Note: CMA-GFS TLM/ADM and CMA-GFS-AERO TLM/ADM are integrated with the same time step (900 s) and the same horizontal resolution of 1°.

Table 6: Computational costs (unit: s) for 6 h integrations of CMA-GFS 4D-Var and CMA-GFS-AERO 4D-Var.

4D-Var system\CPU core	480	960	1440
CMA-GFS 4D-Var	803	515	428
CMA-GFS-AERO 4D-Var	1013	640	591

Note: CMA-GFS 4D-Var and CMA-GFS-AERO 4D-Var are integrated with the same time step of 300 s/900 s (outer loop/inner loop), the same horizontal resolution of 0.25°/1° (outer loop/inner loop), and the same number of minimization iteration of 35 steps.

6 Conclusions

In this study, we developed CMA-GFS-AERO 4D-Var, a strongly coupled aerosol-~~chemistry~~ meteorology data assimilation system, under the framework of the incremental analysis scheme of CMA-GFS 4D-Var. CMA-GFS-AERO 4D-Var includes three ~~component~~ model components: forward, tangent linear, and adjoint models. CMA-GFS-AERO forward model was constructed by integrating the AERO-BC module, an aerosol module containing main aerosol physical processes of BC in the atmosphere, the code of which was extracted from the CUACE air quality model and further optimized in this work, into the CMA-GFS weather model. The tangent linear and the adjoint of the AERO-BC module was developed and coupled online with the TLM and ADM of CMA-GFS, respectively. Thus, CMA-GFS-AERO ADM includes not only the adjoint of physical processes of BC, but also the adjoint of the meteorological model. The BC mass concentration was used as the control variable and minimized together with atmospheric variables. The background error covariance of the control variable BC adopted a modeled structure. The assimilation system used BC surface observations from the China Atmospheric Monitoring Network. The observation error and the observation operator of BC were described in detail as well.

CMA-GFS-AERO TLM and ADM were verified by tangent linear approximation and adjoint correctness test. The results show that CMA-GFS-AERO TLM exhibits good performance in tangent linear approximation for BC, and adjoint sensitivity agrees well with tangent linear sensitivity. The CMA-GFS-AERO 4D-Var system was validated for its accuracy and rationality by the single ~~point~~ observation ~~ideal~~ experiment and the full observation experiment. The results show that assimilating BC observations can generate analysis increments not only for BC but also for atmospheric variables such as temperature, pressure, wind field, and relative humidity. ~~Furthermore, weakly coupled assimilation may amplify the feedback effects of BC assimilation on atmospheric analysis, while the strongly coupled assimilation, constrained by atmospheric observations, does not amplify the feedback effects, highlighting the capability of the CMA-GFS-AERO 4D-Var strongly coupled assimilation system in exploring the feedback effects of BC assimilation on atmospheric variables~~. This demonstrates the successful implementation of the newly developed CMA-GFS-AERO 4D-Var system and highlights it as an effective approach for investigating the feedback of BC data assimilation on meteorological forecasts. Additionally, the computational performance of CMA-GFS-AERO 4D-Var was evaluated, and the results indicate that when using 1440 CPU cores for 6 h integrations, the total time of CMA-GFS-AERO 4D-Var are approximately 1.4 times that of CMA-GFS 4D-Var, highlighting the high efficiency of CMA-GFS-AERO 4D-Var and the potential in operational application.

The next steps are as follows. We intend to explore the impact of assimilating surface BC observations on the forecast fields of BC and atmospheric variables through batch tests. The CMA-GFS-AERO 4D-Var still needs to be applied to control

variables for BC emission scaling factors. Further development of CMA-GFS-AERO 4D-Var will aim to assimilate more aerosol species while ensuring computational efficiency, providing an effective way to study the impact of aerosol assimilation on the analysis and forecast fields of atmospheric variables.

Data and code availability. The CMA-GFS model and its 4D-Var system and CUACE model were distributed by CMA Earth System Modeling and Prediction Centre (CEMC) and the Chinese Academy of Meteorological Sciences (http://www.camscma.cn/), respectively. The model was run on the PI-SUGON high-performance computer with an Intel Fortran Compiler. Due to copyright restrictions of CEMC, the full codes of the system are not freely available, interested users can contact the operational management department of CEMC or the author, Y. Liu (liuyzh@cma.gov.cn), for further assistance. Codes related to this study, including the tangent linear and adjoint interface codes for black carbon (BC), the observation operator codes for BC and the CMA-GFS-AERO 4D-Var main program, are available on Zenodo (https://zenodo.org/records/14880420~~13735640~~; Liu et al., 2024~~5~~). Model outputs of the four assimilation experiments of BC and atmosphere used in this study are also available at this website.

Author contributions. XZ, XS and WH envisioned and oversaw the project. YL and CW developed the model code and performed the simulations. YL, WJ, and CW prepared the manuscript with contributions from all co-authors.

Competing interests. The contact author has declared that none of the authors has any competing interests.

Acknowledgements. This work was supported by Major Program of National Natural Science Foundation of China (42090032). The assimilation and forecast experiments were performed on the high-performance computer Pi-SUGON of China Meteorological Administration. The development of the CMA-GFS-AERO 4D-Var system is a collaborative effort involving contributions from many colleagues~~a systematic project~~. ~~Apart from the authors, many other colleagues have participated in the project.~~ We sincerely thank the entire team for their cooperation. We also thank YaQiang Wang from CAMS for provide anthropogenic emission sources data and black carbon observations.

References

An, X.Q., Zhai, S.X., Jin, M., Gong, S., Wang, Y.: Development of an adjoint model of GRAPES–CUACE and its application in tracking influential haze source areas in north China, Geosci. Model Dev., 9, 2153-2165, https://doi.org/10.5194/gmd-9-2153-2016, 2016.

Arakawa, A., Schubert, W.H.: Interaction of a cumulus cloud ensemble with the large-scale environment, Part I, J. Atmos. Sci., 31, 674-701, https://doi.org/10.1175/1520-0469(1974)031<0674:IOACCE>2.0.CO;2, 1974.

Baklanov, A., Schluenzen, K.H., Suppan, P., Baldasano, J., Zhang, Y.: Online coupled regional meteorology chemistry models in Europe: current status and prospects, Atmos. Chem. Phys., 14, 317-398, https://doi.org/10.5194/acp-14-317-2014, 2014.

Ballard, S. P., Li, Z., Simonin, D., Caron, J. F.: Performance of 4D - Var NWP - based nowcasting of precipitation at the Met Office for summer 2012. Q. J. Roy. Meteor. Soc., 142, 472-487, https://doi.org/10.1002/qj.2665, 2016.

Bergman, K. H.: Multivariate Analysis of Temperatures and Winds Using Optimum Interpolation. Mon. Wea. Rev., 107, 1423–1444, https://doi.org/10.1175/1520-0493(1979)107<1423:MAOTAW>2.0.CO;2, 1979.

Benedetti, A., Morcrette, J.J., Boucher, O., Dethof, A., Engelen, R.J., Fisher, M., Flentje, H., Huneeus, N., Jones, L., Kaiser, J.W.: Aerosol analysis and forecast in the European centre for medium-range weather forecasts integrated forecast system: 2. Data assimilation, J. Geophys. Res.-Atmos., 114, https://doi.org/10.1029/2008JD011115, 2009.

Bocquet, M., Elbern, H., Eskes, H., Hirtl, M., Žabkar, R., Carmichael, G. R., Flemming, J., Inness, A., Pagowski, M., Pérez Camaño, J. L., Saide, P. E., San Jose, R., Sofiev, M., Vira, J., Baklanov, A., Carnevale, C., Grell, G., and Seigneur, C.: Data assimilation in atmospheric chemistry models: current status and future prospects for coupled chemistry meteorology models, Atmos. Chem. Phys., 15, 5325-5358, https://doi.org/10.5194/acp-15-5325-2015, 2015.

Bond, T.C., Doherty, S.J., Fahey, D.W., Forster, P.M., Berntsen, T., DeAngelo, B.J., Flanner, M.G., Ghan, S., Kärcher, B., Koch, D.: Bounding the role of black carbon in the climate system: A scientific assessment, J. Geophys. Res.-Atmos., 118, 5380-5552, https://doi.org/10.1002/jgrd.50171, 2013.

Chen, D., Liu, Z., Ban, J., Zhao, P., Chen, M.: Retrospective analysis of 2015–2017 wintertime PM 2.5 in China: response to emission regulations and the role of meteorology, Atmos. Chem. Phys., 19, 7409-7427, https://doi.org/10.5194/acp-19-7409-2019, 2019.

Chen, D. and Shen, X.: Recent progress on GRAPES research and application, J. Appl. Meteor. Sci., 17, 773-777, 2006 (in Chinese).

Chen, D., Xue, J., Yang, X., Zhang, H., Shen, X., Hu, J., Wang, Y., Ji, L., Chen, J.: New generation of multi-scale NWP system (GRAPES): general scientific design, Chinese Sci. Bull., 53, 3433-3445, https://doi.org/10.1007/s11434-008-0494-z, 2008.

Chen, W., Wang, Y., Li, J., Yi, Z., Zhao, Z., Guo, B., Che, H., Zhang, X.: Description and evaluation of a newly developed emission inventory processing system (EMIPS), Sci. Total Environ., 870, 161909, https://doi.org/10.1016/j.scitotenv.2023.161909, 2023.

Chung, S.H. and Seinfeld, J.H.: Global distribution and climate forcing of carbonaceous aerosols, J. Geophys. Res.-Atmos., 107, AAC 14-11-AAC 14-33, https://doi.org/10.1029/2001JD001397, 2002.

Courtier, P., Thépaut, J.N., Hollingsworth, A.: A strategy for operational implementation of 4D-Var, using an incremental approach, Q. J. Roy. Meteor. Soc., 120, 1367-1387, https://doi.org/10.1002/qj.49712051912, 1994.

Dai, Y., Zeng, X., Dickinson, R. E., Baker, I., Bonan, G. B., Bosilovich, M. G., Denning, A. S., Dirmeyer, P. A., Houser, P. R., Niu, G., Oleson, K. W., Schlosser, C. A., Yang, Z.: The Common Land Model, B. Am. Meteorol. Soc., 84, 1013-1024, https://doi.org/10.1175/BAMS-84-8-1013, 2003.

Elbern, H. and Schmidt, H.: A four-dimensional variational chemistry data assimilation scheme for Eulerian chemistry

transport modeling, J. Geophys. Res.-Atmos., 104, 18583-18598, https://doi.org/10.1029/1999JD900280, 1999.

Elbern, H., Strunk, A., Schmidt, H., Talagrand, O.: Emission rate and chemical state estimation by 4-dimensional variational inversion, Atmos. Chem. Phys., 7, 3749-3769, https://doi.org/10.5194/acp-7-3749-2007, 2007.

Flemming, J., Huijnen, V., Arteta, J., Bechtold, P., Beljaars, A., Blechschmidt, A.M., Diamantakis, M., Engelen, R.J., Gaudel, A., Inness, A.: Tropospheric chemistry in the Integrated Forecasting System of ECMWF, Geosci. Model Dev., 8, 975-1003, https://doi.org/10.5194/gmd-8-975-2015, 2015.

Flemming, J., Inness, A., Jones, L., Eskes, H.J., Huijnen, V., Schultz, M.G., Stein, O., Cariolle, D., Kinnison, D., Brasseur, G.: Forecasts and assimilation experiments of the Antarctic ozone hole 2008, Atmos. Chem. Phys., 11, 1961-1977, https://doi.org/10.5194/acp-11-1961-2011, 2011.

Gelbard, F., Tambour, Y., Seinfeld, J. H.: Sectional representations for simulating aerosol dynamics. J. Colloid Interf. Sci., 76, 541-556, https://doi.org/10.1016/0021-9797(80)90394-X, 1980.

Gong, S.L., Barrie, L.A., Blanchet, J.P., Von Salzen, K., Lohmann, U., Lesins, G., Spacek, L., Zhang, L.M., Girard, E., Lin, H.: Canadian Aerosol Module: A size-segregated simulation of atmospheric aerosol processes for climate and air quality models 1. Module development, J. Geophys. Res.-Atmos., 108, AAC 3-1-AAC 3-16, https://doi.org/10.1029/2001JD002002, 2003.

Gong, S.L. and Zhang, X.Y.: CUACE/Dust–an integrated system of observation and modeling systems for operational dust forecasting in Asia, Atmos. Chem. Phys., 8, 2333-2340, https://doi.org/10.5194/acp-8-2333-2008, 2008.

~~Gong, T., Sun, Z., Zhang, X., Zhang, Y., Wang, S., Han, L., Zhao, D., Ding, D., Zheng, C.: Associations of black carbon and PM2. 5 with daily cardiovascular mortality in Beijing, China, Atmos. Environ., 214, 116876, https://doi.org/10.1016/j.atmosenv.2019.116876, 2019.~~

Granier, C., Darras, S., Gon, H.D.v.d., Jana, D., Elguindi, N., Bo, G., Michael, G., Marc, G., Jalkanen, J.-P., Kuenen, J., Liousse, C., Quack, B., Simpson, D., Sindelarova, K.: The Copernicus Atmosphere Monitoring Service Global and Regional Emissions (April 2019 Version), Copernicus Atmosphere Monitoring Service, 2019.

Guerrette, J.J. and Henze, D.K.: Development and application of the WRFPLUS-Chem online chemistry adjoint and WRFDA-Chem assimilation system, Geosci. Model Dev., 8, 1857 – 1876, https://doi.org/10.5194/gmd-8-1857-2015, 2015.

Guo, B., Wang, Y., Zhang, X., Che, H., Ming, J., Yi, Z.: Long-Term variation of black carbon aerosol in China based on revised aethalometer monitoring data, Atmosphere, 11, 684, https://doi.org/10.3390/atmos11070684, 2020.

Hakami, A., Henze, D.K., Seinfeld, J.H., Singh, K., Sandu, A., Kim, S., Byun, Li, Q.: The adjoint of CMAQ, Environ. Sci. Technol., 41, 7807-7817, https://doi.org/10.1021/es070944p, 2007.

Han, J., Pan, H.L.: Revision of convection and vertical diffusion schemes in the NCEP global forecast system., Wea.

Forecast., 26, 520-533, https://doi.org/10.1175/WAF-D-10-05038.1, 2011.

Henze, D.K., Hakami, A., Seinfeld, J.H.: Development of the adjoint of GEOS-Chem, Atmos. Chem. Phys., 7, 2413-2433, https://doi.org/10.5194/acp-7-2413-2007, 2007.

Henze, D.K., Seinfeld, J.H., Shindell, D.T.: Inverse modeling and mapping US air quality influences of inorganic PM 2.5 precursor emissions using the adjoint of GEOS-Chem, Atmos. Chem. Phys., 9, 5877-5903, https://doi.org/10.5194/acp-9-5877-2009, 2009.

Hong, S.Y., Pan, H.L.: Nonlocal boundary layer vertical diffusion in a medium-range forecast model, Mon. Weather Rev., 124, 2322-2339, https://doi.org/10.1175/1520-0493(1996)124<2322:NBLVDI>2.0.CO;2, 1996.

Huo, Z., Li, X., Chen, J., Liu, Y.: CMA global ensemble prediction using singular vectors from background field, J. Appl. Meteor. Sci., 33, 655-667, 2022 (in Chinese).

Inness, A., Baier, F., Benedetti, A., Bouarar, I., Chabrillat, S., Clark, H., Clerbaux, C., Coheur, P., Engelen, R.J., Errera, Q., Flemming, J., George, M., Granier, C., Hadji-Lazaro, J., Huijnen, V., Hurtmans, D., Jones, L., Kaiser, J.W., Kapsomenakis, J., Lefever, K., Leitão, J., Razinger, M., Richter, A., Schultz, M.G., Simmons, A.J., Suttie, M., Stein, O., Thépaut, J.N., Thouret, V., Vrekoussis, M., Zerefos, C., the, M.t.: The MACC reanalysis: an 8 yr data set of atmospheric composition, Atmos. Chem. Phys., 13, 4073-4109, https://doi.org/10.5194/acp-13-4073-2013, 2013.

Jacobson, M.Z., Turco, R.P., Jensen, E.J., Toon, O.B.: Modeling coagulation among particles of different composition and size, Atmos. Environ., 28, 1327-1338, https://doi.org/10.1016/1352-2310(94)90280-1, 1994.

Janssens-Maenhout, G., Crippa, M., Guizzardi, D., Dentener, F., Muntean, M., Pouliot, G., Keating, T., Zhang, Q., Kurokawa, J., Wankmüller, R.: HTAP_v2. 2: a mosaic of regional and global emission grid maps for 2008 and 2010 to study hemispheric transport of air pollution, Atmos. Chem. Phys., 15, 11411-11432, https://doi.org/10.5194/acp-15-11411-2015, 2015.

Koch, D.: Transport and direct radiative forcing of carbonaceous and sulfate aerosols in the GISS GCM, J. Geophys. Res.-Atmos., 106, 20311-20332, https://doi.org/10.1029/2001JD900038, 2001.

Kuhlbusch, T.A.J.: Black carbon and the carbon cycle. Science, 280, 1903-1904, doi: 10.1126/science.280.5371.1903, 1998.

Lanczos, C.: An iteration method for the solution of the eigenvalue problem of linear differential and integral operators, Journal of Research of the National Bureau of Standards, 45, ,255–282, 1950.

Li, M., Zhang, Q., Kurokawa, J.-i., Woo, J.-H., He, K., Lu, Z., Ohara, T., Song, Y., Streets, D.G., Carmichael, G.R.: MIX: a mosaic Asian anthropogenic emission inventory under the international collaboration framework of the MICS-Asia and HTAP, Atmos. Chem. Phys., 17, 935-963, https://doi.org/10.5194/acp-17-935-2017, 2017.

Liu, F.: Adjoint model of Comprehensive Air quality Model CAMx–construction and application, Post-doctoral research report, Peking University, Beijing, 2005 (in Chinese).

Liu, K., Chen, Q., Sun, J.: Modification of cumulus convection and planetary boundary layer schemes in the GRAPES global model, J. Meteorol. Res., 29, 806-822, https://doi.org/10.1007/s13351-015-5043-5, 2015.

Liu, Q., Hu, Z., Zhou, X.: Explicit Cloud Schemes of HLAFS and Simulation of Heavy Rainfall and Clouds, Part I: Explicit Cloud Schemes., J. Appl. Meteor. Sci., 14, 60-67, 2003a (In Chinese).

Liu, Q., Hu, Z., Zhou, X.: Explicit Cloud Schemes of HLAFS And Simulation of Heavy Rainfall And Clouds, Part II: Simulation of Heavy Rainfall and Clouds., J. Appl. Meteor. Sci., 14, 68-77, 2003b (In Chinese).

Liu, Y., Gong, J., Zhang, L., Chen, Q.: Influence of linearized physical processes on the GRAPES 4DVAR, Acta Meteorol. Sin., 77, 196-209, 2019.

Liu, Y., Zhang, L., Chen, J., Wang, C.: An improvement of the linearized planetary boundary layer parameterization scheme for CMA-GFS 4DVar. J. Appl. Meteor. Sci., 34, 15-26, doi: 10.11898/1001-7313.20230102, 2023.

Liu, Y., Zhang, L., Jin, Z.: The Optimization of GRAPES Global Tangent Linear Model and Adjoint Model. Journal of Applied Meteorological Science, 28, 62-71, doi: 10.11898/1001-7313.20170106, 2017 (in Chinese).

Liu, Y., Zhang, L., Lian, Z.: Conjugate Gradient Algorithm in the Four-Dimensional Variational Data Assimilation System in GRAPES, J. Meteorol. Res., 32, 974-984, https://doi.org/10.1007/s13351-018-8053-2, 2018.

Li, Z., Liu, Q., Ma, Z.: Influences of Graupel Microphysics on CMA-GFS Simulation of Summer Regional Precipitation, J. Meteorol. Res., 38, 27-38, https://doi.org/10.1007/s13351-024-3068-3, 2024.

Lorenc, A.C., Ballard, S.P., Bell, R.S., Ingleby, N.B., Andrews, P.L.F., Barker, D.M., Bray, J.R., Clayton, A.M., Dalby, T., Li, D.: The Met. Office global three-dimensional variational data assimilation scheme, Q. J. Roy. Meteor. Soc., 126, 2991-3012, doi:10.1256/smsqj.57001, 2000.

~~Lorenc, A.C. and Rawlins, F.: Why does 4D-Var beat 3D-Var? Q. J. Roy. Meteor. Soc., 131, https://doi.org/10.1256/qj.05.85, 2010.~~

Mahfouf, J.-F.: Influence of physical processes on the tangent-linear approximation, Tellus A: Dynamic Meteorology and Oceanography, 51, 147-166, https://doi.org/10.3402/tellusa.v51i2.12312, 1999.

Mahfouf, J.F. and Rabier, F.: The ECMWF operational implementation of four-dimensional variational assimilation-Part I : Experimental results with simplified physics, Q. J. Roy. Meteor. Soc., 126, 1143-1170, https://doi.org/10.1002/qj.49712656415, 2000.

Meng, Z., Dabdub, D., Seinfeld, J. H.: Size-resolved and chemically resolved model of atmospheric aerosol dynamics, J. Geophys. Res., 103, 3419–3435, https://doi.org/10.1029/97JD02796, 1998.

Menon, S., Hansen, J., Nazarenko, L., Luo, Y.: Climate effects of black carbon aerosols in China and India, Science, 297, 2250-2253, doi: 10.1126/science.1075159, 2002.

Menut, L., Vautard, R., Beekmann, M., Honoré, C.: Sensitivity of photochemical pollution using the adjoint of a simplified

chemistry-transport model, J. Geophys. Res.-Atmos., 105, 15379-15402, https://doi.org/10.1029/1999JD900953, 2000.

Mlawer, E.J., Taubman, S.J., Brown, P.D., Iacono, M.J., Clough, S.A.: Radiative transfer for inhomogeneous atmospheres: RRTM, a validated correlated-k model for the long wave, J. Geophys. Res.-Atmos., 102, 16663 – 16682, https://doi.org/10.1029/97JD00237, 1997.

Morcrette, J. J., Barker, H.W., Cole, J. N. S., Iacono, M. J., Pincus, R.: Impact of a new radiation package, McRad, in the ECMWF Integrated Forecast System, Mon. Weather Rev., 136, 4773-4798, https://doi.org/10.1175/2008MWR2363.1, 2008.

Müller, J.F. and Stavrakou, T.: Inversion of CO and NO x emissions using the adjoint of the IMAGES model, Atmos. Chem. Phys., 5, 1157-1186, https://doi.org/10.5194/acp-5-1157-2005, 2005.

Pagowski, M., Grell, G. A.: Experiments with the assimilation of fine aerosols using an Ensemble Kalman Filter, J. Geophys. Res., 117, D21302, doi:10.1029/2012JD018333, 2012.

Pagowski, M., Grell, G.A., McKeen, S.A., Peckham, S.E., Devenyi, D.: Three-dimensional variational data assimilation of ozone and fine particulate matter observations: some results using the Weather Research and Forecasting—Chemistry model and Grid-point Statistical Interpolation, Q. J. Roy. Meteor. Soc., 136, 2013-2024, https://doi.org/10.1002/qj.700, 2010.

Sandu, A., Daescu, D.N., Carmichael, G.R., Chai, T.: Adjoint sensitivity analysis of regional air quality models, J. Comput. Phys., 204, 222-252, https://doi.org/10.1016/j.jcp.2004.10.011, 2005.

Schmidt, H. and Martin, D.: Adjoint sensitivity of episodic ozone in the Paris area to emissions on the continental scale, J. Geophys. Res.-Atmos., 108, https://doi.org/10.1029/2001JD001583, 2003.

Schwartz, C.S., Liu, Z., Lin, H.C., McKeen, S.A.: Simultaneous three-dimensional variational assimilation of surface fine particulate matter and MODIS aerosol optical depth, J. Geophys. Res.-Atmos., 117, https://doi.org/10.1029/2011JD017383, 2012.

Seinfeld, J.H. and Pandis, S.N.: Atmospheric Chemistry and Physics: From Air Pollution to Climate Change, Environment ence & Policy for Sustainable Development, 1998.

Semane, N., Peuch, V.H., Pradier, S., Desroziers, G., El Amraoui, L., Brousseau, P., Massart, S., Chapnik, B., Peuch, A.: On the extraction of wind information from the assimilation of ozone profiles in Météo–France 4-D-Var operational NWP suite, Atmos. Chem. Phys., 9, 4855-4867, https://doi.org/10.5194/acp-9-4855-2009, 2009.

Shen, X., Su, Y., Zhang, H., Hu, J.: New Version of the CMA-GFS Dynamical Core Based on the Predictor–Corrector Time Integration Scheme, J. Meteorol. Res., 37, 273-285, https://doi.org/10.1007/s13351-023-3002-0, 2023.

Smith, P. J., Fowler, A. M., Lawless, A. S.: Exploring strategies for coupled 4D-Var data assimilation using an idealised atmosphere – ocean model. Tellus A: Dynamic Meteorology and Oceanography, 67, 27025,

https://doi.org/10.3402/tellusa.v67.27025, 2015.

Su, Y., Shen, X., Peng, X., Li, X., Wu, X., Zhang, S., Chen, X.: Application of PRM scalar advection scheme in GRAPES global forecast system, Chinese Journal of Atmospheric Sciences, 37, 1309-1325, doi:10.3878/j.issn.1006-9895.2013.12164, 2013 (in Chinese).

Tian, X. and Zou, X.: Development of the tangent linear and adjoint models of the MPAS-Atmosphere dynamic core and applications in adjoint relative sensitivity studies, Tellus A:Dynamic Meteorology and Oceanography, 72, 16, https://doi.org/10.1080/16000870.2020.1814602, 2020.

Vautard, R., Beekmann, M., Menut, L.: Applications of adjoint modelling in atmospheric chemistry: sensitivity and inverse modelling, Environ. Modell. Softw., 15, 703-709, https://doi.org/10.1016/S1364-8152(00)00058-X, 2000.

Wang, C., An, X., Zhao, D., Sun, Z., Jiang, L., Li, J., Hou, Q.: Development of GRAPES-CUACE adjoint model version 2.0 and its application in sensitivity analysis of ozone pollution in north China, Sci. Total Environ., 826, 153879, https://doi.org/10.1016/j.scitotenv.2022.153879, 2022.

Wang, H., Gong, S., Zhang, H., Chen, Y., Shen, X., Chen, D., Xue, J., Shen, Y., Wu, X., Jin, Z.: A new-generation sand and dust storm forecasting system GRAPES_CUACE/Dust: Model development, verification and numerical simulation, Chin. Sci. Bull., 55, 635-649, https://doi.org/10.1007/s11434-009-0481-z, 2010.

Wang, H., Peng, Y., Zhang, X., Liu, H., Zhang, M., Che, H., Cheng, Y., Zheng, Y.: Contributions to the explosive growth of PM 2.5 mass due to aerosol–radiation feedback and decrease in turbulent diffusion during a red alert heavy haze in Beijing–Tianjin–Hebei, China, Atmos. Chem. Phys., 18, 17717-17733, https://doi.org/10.5194/acp-18-17717-2018, 2018.

Xu, X., Yang, X., Zhu, B., Tang, Z., Wu, H., Xie, L.: Characteristics of MERRA-2 black carbon variation in east China during 2000–2016, Atmos. Environ., 222, 117140, https://doi.org/10.1016/j.atmosenv.2019.117140, 2020.

Yang, X., Chen, J., Hu, J., Chen, D., Shen, X., Zhang, H.: A semi-implicit semi-Lagrangian global nonhydrostatic model and the polar discretization scheme, Sci. China Ser. D, 50, 1885-1891, https://doi.org/10.1007/s11430-007-0124-7, 2007.

Zhang, L., Liu, Y., Liu, Y., Gong, J., Lu, H., Jin, Z., Tian, W., Liu, G., Zhou, B., Zhao, B.: The operational global four-dimensional variational data assimilation system at the China Meteorological Administration, Q. J. Roy. Meteor. Soc., 145, 1882-1896, https://doi.org/10.1002/qj.3533, 2019.

Zhang, Y.: Online-coupled meteorology and chemistry models: history, current status, and outlook, Atmos. Chem. Phys., 8, https://doi.org/10.5194/acp-8-2895-2008, 2008.

Zheng, B., Tong, D., Li, M., Liu, F., Hong, C., Geng, G., Li, H., Li, X., Peng, L., Qi, J.: Trends in China's anthropogenic emissions since 2010 as the consequence of clean air actions, Atmos. Chem. Phys., 18, 14095-14111, https://doi.org/10.5194/acp-18-14095-2018, 2018.

Zhou, C., Gong, S., Zhang, X., Liu, H., Xue, M., Cao, G., An, X., Che, H., Zhang, Y., Niu, T.: Towards the improvements of

simulating the chemical and optical properties of Chinese aerosols using an online coupled model–CUACE/Aero, Tellus B: Chemical and Physical Meteorology, 64, 18965, https://doi.org/10.3402/tellusb.v64i0.18965, 2012.

Zhu, S., Wang, B., Zhang, L., Liu, J., Liu, Y., Gong, J., Xu, S., Wang, Y., Huang, W., Liu, L., He, Y., Wu, X., Zhao, B., Chen, F.: A 4DEnVar-based ensemble four-dimensional variational (En4DVar) hybrid data assimilation system for global NWP: system description and primary tests., J. Adv. Model. Earth Sy., 14(8), https://doi.org/10.1029/2022MS003023, e2022MS003023, 2022.

Zou, X., Vandenberghe, F., Pondeca, M. and Kuo, Y.-H.: Introduction to adjoint techniques and the MM5 adjoint modeling system (No. NCAR/TN-435 þ STR). University Corporation for Atmospheric Research. 1997.